Supplementary Material

Two-step interrogation then recognition of DNA binding site by Integration Host Factor: an architectural DNA-bending protein

Yogambigai Velmurugu[1], Paula Vivas[1,†], Mitchell Connolly[1], Serguei V. Kuznetsov[1], Phoebe A. Rice[2] and Anjum Ansari[1,3*]

[1]Department of Physics, University of Illinois at Chicago, Chicago, IL 60607, USA;
[2]Department of Biochemistry & Molecular Biology, University of Chicago, Chicago IL 60637, USA;
[3]Department of Bioengineering, University of Illinois at Chicago, Chicago, IL 60607, USA;

[†] Present address: ASK Chemicals, 5200 Blazer Parkway, Dublin, OH 43017

* To whom correspondence should be addressed
Telephone: (312) 996-8735, Fax:(312) 996-9016 Email: ansari@uic.edu

Supplementary Methods

1.1 Materials. All labeled and unlabeled DNA oligonucleotides were purchased with gel purification from the Keck Foundation (Yale University). DNA concentration for each strand (prior to making duplex DNA) was determined by measuring the absorbance at 260 nm, with extinction coefficients 4.0×10^5 $M^{-1}cm^{-1}$ for the F-labeled (top) strand and 4.15×10^5 $M^{-1}cm^{-1}$ for the R-labeled (bottom) strand. To determine the extent of labeling in each strand, fluorescein and TAMRA concentrations were obtained independently for each of the labeled strands using absorbance of F-labeled strands at 494 nm and R-labeled strands at 565 nm; these concentrations were compared with those of the oligomers obtained from measurements at 260 nm. For the dyes, the molar extinction coefficients used were 75,000 $M^{-1}cm^{-1}$ for F-dT at 494 nm, and 91,000 $M^{-1}cm^{-1}$ for R-dT at 565 nm, as obtained from Molecular Probes (www.glenresearch.com/Technical/Extinctions.html). The percentage of labeled DNA in solution was estimated to be >95%.

Equimolar concentrations of the upper and lower strands in an annealing buffer (20 mM Tris-HCl, pH 8.0, 1 mM EDTA, and the desired [salt]: 50-200 mM KCl) were mixed and heated in a water bath at 95 ˚C for 5 min and then allowed to cool slowly to room temperature for complete annealing. The IHF protein was prepared as described previously (1). IHF concentration was determined by measuring absorbance at 276 nm, with extinction coefficient 5800 $M^{-1}cm^{-1}$ (2).

1.2 Equilibrium FRET and anisotropy measurements. For each experimental condition, identical samples were prepared but with either donor-only labeled DNA or with donor-acceptor labeled DNA. In each case, the donor (fluorescein) was excited at 485 nm, and the emission spectra were collected from 500 nm to 650 nm. The FRET efficiency (*E*) between fluorescein and TAMRA for a given double-labeled sample was computed using $E = 1 - I_{DA}/I_D$, where I_D and I_{DA} are the donor intensities of the donor-only and donor-acceptor samples, respectively, obtained by computing the area under the donor emission spectra, from 505 nm to 535 nm.

Steady-state anisotropy measurements were performed on donor-acceptor labeled H' DNA, in the presence and absence of IHF, at 20 °C. For anisotropy measurements on the donor (fluorescein), the samples were excited at 485 nm, and the fluorescence emission intensities were collected at 520 nm; for corresponding measurements on the acceptor (TAMRA), the samples were excited at 555 nm, and the fluorescence emission intensities were collected at 580 nm. For each set of measurements, the emission intensities for the parallel ($I_\parallel$) and perpendicular ($I_\perp$) orientations were collected using an integration time of 1 s, and the data were processed using a program provided by Horiba to obtain anisotropy values, defined as: $r = \frac{I_\parallel - I_\perp}{I_\parallel + 2I_\perp}$. The errors in the measured anisotropy were calculated as standard deviations from the average of five independent sets of measurements.

1.3 Circular dichroism measurements. The thermal stability of the IHF protein was measured in the absence and presence of H' DNA, using far-UV circular dichroism (CD) measurements at 222 nm, in the temperature range 15–85 °C. Two sets of measurements were carried out for IHF (30 μM protein concentration), IHF-H' (12.5:15 μM protein:DNA concentration), and H' DNA only (15 μM). Under these conditions, the CD signal for the DNA only at 222 nm was 3.2 ± 0.1 mdeg at 20 °C compared with –15.3 ± 0.1 mdeg for the IHF-H' complex and was weakly dependent on temperature, decreasing to 2.6 ± 0.2 mdeg at 85 °C. The DNA contribution was subtracted from the CD signal of the IHF-H' complex prior to further analysis. The CD measurements for the complex were found to be reversible after heating up to at least 60 °C.

The thermal unfolding profiles were analyzed in terms of a two-state van't Hoff transition with linear upper and lower baselines using the following equation:

$$A(T) = A_L(T) + [A_U(T) - A_L(T)]f_U \quad \text{(S1)}$$

where $A(T)$ is the CD signal of the IHF-H' complex minus the CD signal of H'-DNA alone, $A_L(T)$ and $A_U(T)$ are the lower and upper baselines, respectively, parameterized as straight lines, and f_u is the fraction of unfolded molecules, written in terms of the van't Hoff parameters as:

$$f_u = \frac{A(T)-A_L(T)}{A_U(T)-A_L(T)} = \left(1 + \exp\left[-\frac{\Delta H_{vH}}{R\left(\frac{1}{T}-\frac{1}{T_m}\right)}\right]\right)^{-1} \quad \text{(S2)}$$

In Eq. S2, ΔH_{vH} is the van't Hoff enthalpy change for the unfolding transition, and T_m the corresponding melting temperature.

The fraction of unfolded molecules as a function of temperature obtained from the van't Hoff analysis are shown in Supplementary Figure S2. The uncertainties in the computed fractions, as well as in the reported T_m values, are the standard deviations from fits to two independent sets of CD measurements. The results are overlaid on top of previous studies of IHF and IHF-H' complex stabilities, from Vivas et al. (1), measured using Tyr fluorescence, as well as previous absorbance melting measurements of the H' DNA alone (Supplementary Figure S2B).

1.4 Laser temperature-jump (T-jump) measurements. The home-built laser T-jump spectrometer (3-5) uses 10-ns IR laser pulses at 1550 nm, generated by Raman shifting the 1064 nm pulses from the output of an Nd:YAG laser, which are focused to ~1 mm spot size onto a 2-mm wide sample cuvette of path length 0.5 mm. Each laser pulse (~40 mJ/pulse at the sample position) yields ~5–10 °C T-jump at the center of the heated volume. A continuous wave (cw) output from a 488 nm diode laser (Newport PC13589) was used as a probe source for exciting the donor (fluorescein), and was focused to a ~100 μm spot in the middle of the heated volume (3). The fluorescence emission intensities of the donor were monitored perpendicular to the excitation direction, with a broad-band filter centered at 536 nm and a 40 nm bandwidth (Semrock FF01-536/40-25), and measured with a Hamamatsu R928 photomultiplier tube. All T-jump measurements carried out in 100 mM KCl were digitized with a 500 MHz transient digitizer (Hewlett Packard 54825A); data for the other salt conditions,

measured at a later time, were digitized with a different 500 MHz digitizer (Tektronix DP04054B). For each experiment, 512 kinetic traces were acquired and averaged by the digitizer. The time interval between subsequent laser pulses was kept at 1 s, to allow sufficient time for the temperature of the heated volume to decay back to that of the surrounding sample holder (maintained at the initial temperature by a water bath circulator) before the arrival of the next laser pulse.

1.5 Acquisition of T-jump kinetics traces. To acquire data with the highest temporal resolution and be able to span several orders of magnitudes in time scale, we measured T-jump kinetics traces over different time-scales and then combined these traces. We typically acquired the kinetics traces on at least two time scales. For measurements with the Hewlett Packard digitizer, data collected on each time scale consisted of 20,000 points; the short time-scale covered kinetics up to 1.6 ms, with a time-resolution of 80 ns, while the longer time-scale covered kinetics up to 40 ms, with a time-resolution of 2 μs. The data acquired in each time-scale were reduced to 10,000 points by averaging 2 points together in each case. For measurements with the Tektronix digitizer, data collected on each time scale consisted of 1 million points, which were reduced to 10,000 points by averaging 100 points together. After averaging, the time interval between data points was 160 ns and 4 μs for the short and long time-scale data, respectively. Prior to any further analysis, data acquired below ~20 μs in each trace were discarded because of artifacts either from scattered infrared laser light into the photomultiplier tube, or due to cavitation effects from microbubbles in the samples (6). Relaxation traces acquired over different timescales were combined as described below.

1.6 Matching of kinetics traces measured over different time scales. Relaxation kinetics traces measured over two different time scales were fitted simultaneously to double-exponential decay convoluted with the T-jump recovery kinetics (see Supplementary Methods 1.9):

$$I(t) = \big(I(0^+) - I(\infty)\big)[f_1 \exp(-k_1 t) + (1 - f_1)\exp(-k_2 t)] + \big(I(\infty) - I(0^-)\big)\left(\frac{1}{1+t/\tau_{rec}}\right) + I(0^-) \quad \text{(S3)}$$

Here $I(0^-)$ is the intensity prior to the *T*-jump, $I(0^+)$ is the initial intensity measured immediately after *T*-jump, $I(\infty)$ is the intensity expected at the end of the conformational relaxation, prior to the recovery of the T-jump itself (see section 1.9), τ_{rec} is a characteristic time constant for the T-jump recovery, k_1 is the relaxation rate for the fast phase, with fractional amplitude f_1, and k_2 is the relaxation rate for the second (slow) phase, with fractional amplitude $f_2 = 1 - f_1$. The following parameters were varied to obtain the best fit: $I(0^+)$, $I(\infty)$, k_1, k_2, and f_1, with τ_{rec} fixed from measurements on control samples. An additional fitting parameter served as a multiplicative scale factor applied to one of the traces to account for any systematic difference in the measured intensities between the two traces (7,8). Once

appropriately scaled, the multiple data sets were combined into a single kinetic trace that covered the time range from 20 μs to 16-40 ms.

1.7 Monte-Carlo search in parameter space for discrete exponential and data matching analysis. To examine whether the scaling and matching of the relaxation traces from the two separate time-scales were indeed robustly done, we carried out a Monte-Carlo search in parameter space using a simulated annealing procedure to minimize the residuals, as described previously (9-11). The parameters were randomly chosen from a wide range and the residuals were minimized by simulated annealing. Each set of parameters obtained by this procedure was then used as starting values for minimization using a least-squares non-linear fitting procedure implemented in MATLAB (R2014A 8.3.0.532). This fitting procedure was repeated with 30 independent randomly chosen sets as starting points. All 30 sets converged to the same global minimum after the non-linear least-squares minimization step. Rates and amplitudes from these best fit set are shown for the IHF-H' complex in Supplementary Figure S6A,B, and for the IHF-TT8AT complex in Supplementary Figure S11A,B, for two independent sets of T-jump measurements. The uncertainties σ_{MC} in each of these parameters for each data set are calculated as the weighted standard deviation from the outputs at the end of the simulated annealing procedure, as follows:

$$\sigma_{MC}^2 = \sum_{i=1}^{30} \frac{(p_i - p_{best})^2}{\chi_i^2} \quad \text{(S4)}$$

where p_i is the value of a given parameter in the *i*-th fit, χ_i^2 is the corresponding residual chi-square for that fit, and p_{best} is the best-fit value of that parameter obtained from the non-linear least-squares minimization. The results from the two independent data sets were then averaged together to get the combined best-fit values for each of the parameters, and the corresponding uncertainties in the parameters for the combined data sets σ_c were computed as follows:

$$\sigma_c^2 = \frac{\sigma_{MC,1}^2 + \sigma_{MC,2}^2}{4} \quad \text{(S5)}$$

These rates and amplitudes averaged over the two data sets are shown for IHF-H' in Supplementary Figure S6C,D and for IHF-TT8AT in Supplementary Figure S11C,D.

1.8 Estimating the size of the T-jump. The magnitude of the T-jump in each relaxation trace was determined by comparing the initial change in donor fluorescence, measured immediately after the T-jump, with equilibrium measurements of the temperature dependence of the donor quantum yield, measured on a reference sample such as donor-only labeled strand of DNA or donor-acceptor-labeled DNA in the absence of IHF, as illustrated in Supplementary Figure S4.

We note here that in our T-jump spectrometer, the IR pulse that heats the sample is incident from only one side of our sample cuvette, which results in a nonuniform T-jump across the 0.5 mm pathlength of the cuvette. An average T-jump of 5 ℃ over a 0.5 mm path length cuvette is estimated to span ~6.5℃ T-jump at the near edge of the sample to ~3.5℃

at the far edge (12,13). This range corresponds to ~30% error in the estimated final temperature T_f, which is approximately the size of the symbols used in our Arrhenius plots; we have therefore not included these errors in explicitly in our plots. We further note that, despite this temperature gradient across the sample, our initial T-jump studies on the IHF-H' complexes, that were done using both 0.5 mm and 1 mm pathlength cells, demonstrated good overlap between the relaxation rates measured as a function of T_f, well within the uncertainties in the measured rates from each sample cell (13). These initial studies indicated that the temperature nonuniformity, which is significantly worse in the 1 mm cells and far from ideal, did not severely impact our ability to obtain an average relaxation trace, averaged over the range of T_f, spanning the cuvette.

1.9 Control measurements to obtain T-jump recovery kinetics. The characteristic decay curves that best describe the recovery of the T-jump back to the initial temperature were obtained from measurements on control (donor-labeled stand of DNA or free fluorescein) samples. To obtain a complete profile of the T-jump recovery kinetics, measurements were performed over a time-window up to about 400 ms. A typical recovery profile is shown in Supplementary Figure S3A, which was fitted to the following "T-jump recovery" function:

$$I(t) = \left(I(0^+) - I(0^-)\right)\left(\frac{1}{1+t/\tau_{rec}}\right) + I(0^-) \qquad \text{(S6)}$$

The parameters varied to obtain the best fit to the T-jump recovery traces are $I(0^+)$ and τ_{rec}. $I(0^-)$ is determined from the average of the measured intensities prior to the arrival of the infrared heating pulse. The scatter in the recovery time constants measured on control samples over a range of initial and final temperatures is shown in Supplementary Figure S3C**,** with an average value of 206 ± 24 ms.

1.10 Maximum entropy analysis of relaxation traces. All relaxation traces were analyzed with the maximum entropy method (MEM), using an algorithm provided to us by Dr. Pete Steinbach of the National Institutes of Health (described in refs. (14-16)). The MEM approach has several advantages over discrete exponential analysis to fit relaxation traces. It provides a more robust way to interpret incomplete and noisy data than discrete exponential analysis, which can result in comparable fits to the relaxation traces even with significantly different parameters (amplitudes and relaxation rates). It also provides a model independent description of the relaxation traces in terms of a distribution of relaxation times without *a priori* assumptions as to the number of discrete exponentials required.

The MEM analysis yields a distribution *f*(log τ), which reflects the probability density in logarithmic scale for a given relaxation time τ (Supplementary Figure S1C), that best fits the relaxation kinetics while maximizing the entropy *S*, defined as:

$$S(f,F) = \sum_{j=1}^{M}\left[f_j - F_j - f_j \ln(f_j / F_j)\right] \qquad \text{(S7)}$$

where f_j are the discretized values of the probability density distribution $f(\log \tau)$ and F is a model distribution that is the default distribution in case of noisy data and is assumed to be uniform and flat.

The MEM analyses on our data typically revealed two distinct peaks, indicating deviations from single-exponential decay (Supplementary Figure S1). In cases where the two peaks were reasonably well separated (e.g. Supplementary Figures S9E and S12F), we computed an average relaxation time $\tau_{ave} = 10^{<\log\tau>}$ for each phase, where $<\log\tau>$ is computed from the distribution of relaxation times within each peak, and defined as:

$$<log\boldsymbol{\tau}> = \frac{\sum_{j=1}^{M} log\tau_j \, f(log\tau_j) dlog\tau_j}{\sum_{j=1}^{M} f(log\tau_j) dlog\tau_j} \quad \text{(S8)}$$

If there was some overlap between the peaks (e.g. Supplementary Figures S9F and S12E), the probability density distribution $f(\log\tau)$ was fitted to the sum of two Gaussian distributions, and the average $<\log\tau>$ was obtained from the peak position of each Gaussian distribution. The area under each peak reflects the fractional amplitude in that relaxation phase.

1.11 Accuracy of fast (~100 μs) and slow (~20 ms) relaxation rates measured with T-jump. We note here that while the first time point resolved in our T-jump apparatus is ~20 μs after the IR laser pulse arrives at the sample position, the relaxation rates reported for the fast phase are typically 1×10^4 s^{-1} (~100 μs) and, for some complexes, even faster (see Arrhenius plots in Figures 3, 4, and 8 of the main text). For kinetics phases with relaxation times of 100 μs, the intensities measured in the T-jump apparatus would have already decayed by about 18% within the first 20 μs, which limits the accuracy with which we can ascertain these fast rates. The degree of uncertainty in our fast rates is captured by the variations in these rates from one set of measurements to another, obtained from MEM analyses, which indicate that the fast phase rates appearing at around $1–2\times10^4$ s^{-1} (relaxation times of ~50–100 μs) vary up to at least 2-fold (main text Figures 3A and 4A,C,E); for even faster rate constants (> 2×10^4 s^{-1} as in Figure 4C at low temperatures), the uncertainties are nearly 3-fold. These uncertainties are further magnified if we examine the reproducibility of the rates obtained from conventional double-exponential analyses (Supplementary Figures S6A,C and S11A,C), although these variations also reflect the errors inherent in the discrete exponential analysis approach that are somewhat mitigated in the MEM approach.

At the other end, at times greater than a few milliseconds, we start to have distortions in the relaxation traces from the recovery of the T-jump itself. For a typical T-jump recovery time constant $\tau_{rec} \approx 200$ ms in our set-up, the intensity $I(\infty)$ characteristic of the intensity at the end of the relaxation phases (see Eq. S3) would have already decayed towards the pre-flash level $I(0^-)$ by ~5%, 9%, and 20% at 10, 20, and 50 ms, respectively, as estimated using Eq. S6. The contribution of the T-jump recovery to the overall shape of the relaxation traces also depends on the amplitude of the recovery component $(I(\infty) - I(0^-))$ when compared with the amplitude of the relaxation kinetics itself $(I(\infty) - I(0^+))$. For example, this distortion is expected to be small for the relaxation trace shown in Supplementary Figure S4E but quite significant for the trace shown in Supplementary Figure S4F. For IHF-H' in 100 mM KCl, the

recovery amplitude is ~44–58% of the relaxation kinetics amplitude at low temperature T-jump conditions, and ~13–17% at the high temperature T-jump conditions; therefore, the distortions in the relaxation traces at ~20 ms are expected to be 4–5% at low temperatures and ~1–2% at high temperatures; the corresponding distortions at 50 ms are expected to be 9–12% at low temperatures and 2–4% at high temperatures. We note here that while we explicitly took into account the T-jump recovery contributions to the measured relaxation traces in the double-exponential fits analysis (Eq. S3), the MEM analysis as applied here did not take into consideration these distortions. Therefore, MEM distributions that extend beyond ~10-20 ms do have contributions from the T-jump recovery, although these distortions are ~10% even at 50 ms, as estimated above. Furthermore, a comparison of the slow phase rates from MEM versus double-exponential fits as shown in Supplementary Figure S6C yield reasonably good agreement even for the lowest temperature, slowest rates observed at ~50 s^{-1} (20 ms), indicating that relaxation times up to ~20 ms are recovered with reasonably good accuracy in our measurements, despite the caveats from distortions introduced by T-jump recovery kinetics.

1.12 Arrhenius fits to relaxation rates versus temperature. Two independent sets of measurements were carried out for each sample over a range of initial and final temperatures. Before carrying out the Arrhenius fits on the ln(rate) versus inverse temperature plots, the relaxation rates (and amplitudes) obtained for a given final temperature (T_f), from each set, were averaged together. Although the initial temperatures (T_i) can be controlled to be identical (or close) for the two sets of measurements, the final temperatures obtained from both sets need not overlap, in part because the magnitude of the T-jump depends on the particular spectrometer alignment for that day, and also fluctuates slightly within the day. Therefore, prior to averaging, the rates and amplitudes for each set of measurements were interpolated on to a common grid for T_f, using a linear interpolation on an Arrhenius plot of ln(rates) versus $1/T_f$. The data from the two sets were averaged together on the same Arrhenius scale. The errors in the averaged quantities (rates and amplitudes) are the standard deviations from the two sets.

The averaged ln(rates) versus $1/T_f$ thus generated were fitted to the following Arrhenius equation:

$$\ln(k) = \ln(A) - E_a/RT_f \tag{S9}$$

where E_a is the activation enthalpy, and *R* is the universal gas constant. The errors in the activation energy values reported in the text are standard deviations of the E_a values obtained from each set independently.

1.13 Control experiments to rule out contributions to the relaxation kinetics from dye dynamics. A series of control experiments were performed to rule out any contributions from dye interactions and/or dye dynamics to the observed relaxation kinetics. (1) For any FRET-labeled sample, corresponding measurements were done on donor-only labeled samples to ensure that the observed kinetics were from FRET changes and not from interactions of the

donor (fluorescein) dye with either the DNA or the protein. No kinetics were observed on any of the donor-only samples other than the slow T-jump recovery kinetics (Supplementary Figure S7A), similar to those observed on control measurements done using either a fluorescein-labeled single strand of the H' DNA or with free fluorescein dye (see control experiments shown in all T-jump kinetics figures). These measurements also confirmed the absence of any photo bleaching of the fluorescein dye in the window of the T-jump measurements. (2) To rule out any contribution to the observed kinetics from interactions of the acceptor (TAMRA) dye, T-jump experiments were carried out on FRET-labelled IHF-H' complex by directly exciting TAMRA (at 532 nm, where fluorescein does not absorb) and measuring the temporal response of the fluorescence emission of TAMRA. Again, no relaxation kinetics were observed (Supplementary Figure S7B), thus confirming that interactions of the acceptor dye with the DNA or the protein do not interfere with the observed relaxation kinetics. (3) To examine whether there were any T-jump induced changes in the relative orientation of the dyes attached to the DNA that were not related to an overall change in the DNA conformation, we carried out T-jump measurements on FRET-labeled DNA only samples. For these measurements we designed a shorter 14 bp DNA oligomer labelled with fluorescein and TAMRA, with the sequence context of each of the dyes identical to that in the longer H' sequence (see Supplementary Figure S7D). Note that in this 14 bp sequence, the four nucleotides at the ends, next to the dyes, are the same as in the original H' sequence. The reason for this shorter sequence is that the end-to-end distance in the 35-bp H' sequence is too long for there to be any significant FRET between the dyes without the bound protein. By design, the FRET value in the 14-bp DNA is ~0.5, close to the FRET of H' when bound to IHF, and in a region where small changes in the distance or relative orientation of the dyes would result in a detectable FRET change. Once again, T-jump measurements on this DNA sample did not reveal kinetics other than the T-jump recovery kinetics (Supplementary Figure S7C). Thus, we see no evidence of dye reorientational dynamics in DNA only samples contributing to the observed relaxation kinetics. (4) To further rule out interactions of the dyes with protein, we carried out measurements with longer (55-bp) DNA containing the H' sequence, to increase the distance between the dyes, attached at the ends, and the protein. The data with the 55-bp H' construct are shown in Supplementary Figure S8 together with data on the 35-bp H' construct. The nature of the biphasic kinetics appears unchanged even with the longer DNA. These measurements indicate that interactions of the dyes with the protein are not contributing to the fast phase.

Supplementary References

1. Vivas, P., Velmurugu, Y., Kuznetsov, S.V., Rice, P.A. and Ansari, A. (2012) Mapping the Transition State for DNA Bending by IHF. *J Mol Biol*, **418**, 300-315.
2. Lynch, T.W., Read, E.K., Mattis, A.N., Gardner, J.F. and Rice, P.A. (2003) Integration host factor: putting a twist on protein-DNA recognition. *J. Mol. Biol.*, **330**, 493-502.
3. Kuznetsov, S.V., Kozlov, A.G., Lohman, T.M. and Ansari, A. (2006) Microsecond Dynamics of Protein-DNA Interactions: Direct Observation of the Wrapping/Unwrapping Kinetics of Single-Stranded DNA around the *E. coli* SSB Tetramer. *J. Mol. Biol.*, **359**, 55-65.
4. Kuznetsov, S.V., Sugimura, S., Vivas, P., Crothers, D.M. and Ansari, A. (2006) Direct observation of DNA bending/unbending kinetics in complex with DNA-bending protein IHF. *Proc. Natl. Acad. Sci. USA*, **103**, 18515-18520.
5. Vivas, P., Kuznetsov, S.V. and Ansari, A. (2008) New insights into the transition pathway from nonspecific to specific complex of DNA with Escherichia coli integration host factor. *J Phys Chem B*, **112**, 5997-6007.
6. Wray, W.O., Aida, T. and Dyer, R.B. (2002) Photoacoustic cavitation and heat transfer effects in the laser-induced temperature jump in water. *Appl. Phys. B*, **74**, 57-66.
7. Velmurugu, Y. (2016), Dynamics and mechanism of DNA-bending proteins in binding-site recognition. Ph.D. thesis. University of Illinois at Chicago, Chicago.
8. Velmurugu, Y., Chen, X., Slogoff Sevilla, P., Min, J.H. and Ansari, A. (2016) Twist-open mechanism of DNA damage recognition by the Rad4/XPC nucleotide excision repair complex. *Proc Natl Acad Sci U S A*, **113**, E2296-2305.
9. Metropolis, N., Rosenbluth, A.W., Rosenbluth, M.N., Teller, A.H. and Teller, E. (1953) Equation of state calculations by fast computing machines. *J. Chem. Phys.*, **21**, 1087-1092.
10. Ansari, A., Jones, C.M., Henry, E.R., Hofrichter, J. and Eaton, W.A. (1994) Conformational relaxation and ligand binding in myoglobin. *Biochemistry*, **33**, 5128-5145.
11. Kuznetsov, S.V., Shen, Y., Benight, A.S. and Ansari, A. (2001) A semiflexible polymer model applied to loop formation in DNA hairpins. *Biophys. J.*, **81**, 2864-2875.
12. Kubelka, J. (2009) Time-resolved methods in biophysics. 9. Laser temperature-jump methods for investigating biomolecular dynamics. *Photochem. Photobiol. Sci.*, **8**, 499-512.
13. Vivas, P. (2009), Mechanism of integration host factor, a DNA-bending protein, probed with laser temperature-jump. Ph.D. thesis. University of Illinois at Chicago, Chicago.
14. Livesey, A.K. and Brochon, J.C. (1987) Analyzing the Distribution of Decay Constants in Pulse-Fluorimetry Using the Maximum Entropy Method. *Biophys J*, **52**, 693-706.
15. Steinbach, P.J., Ionescu, R. and Matthews, C.R. (2002) Analysis of kinetics using a hybrid maximum-entropy/nonlinear-least-squares method: application to protein folding. *Biophys J*, **82**, 2244-2255.
16. Steinbach, P.J. (2002) Inferring lifetime distributions from kinetics by maximizing entropy using a bootstrapped model. *J Chem Inf Comput Sci*, **42**, 1476-1478.

Supplementary Figure Legends:

Figure S1. **Matching kinetic traces measured on two separate time scales and maximum entropy analysis of the combined relaxation trace.** (**A**) Kinetics traces taken on two separate time-scales are shown: full time-scale 1.6 ms (magenta) and full time scale 16 ms (blue). The black lines through the kinetics traces are a fit to the data using the two-exponential decay function and a scale factor to account for the difference in intensities between the two traces. (**B**) The kinetics trace obtained after matching and combining the two traces shown in (**A**), as described in Supplementary Methods 1.6. The continuous red line is from a fit to the data using the maximum entropy analysis. (**C**) The distribution of the log of the relaxation times, log(τ), that best describes the relaxation trace in (**B**) is shown (red). The blue line represents a fit to the distribution in terms of two Gaussians (shown in green), with independently varied peak positions and widths. The range of the distribution that falls outside the time-scales of the measured relaxation trace is shown as dashed lines.

Figure S2. Thermal melting profiles of IHF with and without bound H' DNA substrate. (**A**) The normalized change in ellipticity at 222 nm is plotted as a function of temperature for IHF (30 μM; gray circles) and IHF-H' (12.5 μM:15 μM; purple triangles). The continuous lines are a fit to the melting profiles using a two-state van't Hoff relation for fraction unfolded that yield the melting temperatures (T_m) of 55.9 ± 1.5 °C and 70.8 ± 0.8 °C, respectively. (**B**) The data shown in panel (**A**) are plotted together with previous measurements of IHF stability, from Vivas et al. (1): (red circles) ellipticity of IHF (30 μM) at 276 nm ($T_m \approx 58$°C); (blue circles) Tyr fluorescence intensity in IHF (10 μM) at 310 nm, with excitation at 276 nm ($T_m \approx 57$°C); (green triangles) Tyr fluorescence emission intensity in IHF-H' (5 μM:5 μM) complex ($T_m \approx$ 70°C); and (black squares) absorbance of H' substrate (4.5 μM) at 266 nm ($T_m \approx 68$°C). All measurements were in 100 mM KCl.

Figure S3. T-jump measurements on donor-only labeled ssDNA control sample. (**A**) Representative relaxation trace measured on donor-only labeled ssDNA (5 μM) after a ~4 °C T-jump is shown. The continuous line is a fit to the T-jump recovery function (Eq. S6), which yields the recovery time constant $\tau_{rec} = 208$ ms. (**B**) The magnitude of the T-jump (ΔT) is plotted versus the initial temperature for a series of control measurements on this sample. The average T-jump from this set is 5.6 ± 0.2 °C. (**C**) The recovery time constant τ_{rec} values obtained from a series of control measurements are plotted as a function of initial temperature. The average value for τ_{rec} from this set is 206 ± 24 ms.

Figure S4. Magnitude of T-jump and amplitude of relaxation in the T-jump relaxation traces. (**A,B**) Equilibrium measurements of the donor fluorescence emission intensity versus temperature are shown for the donor-acceptor labeled IHF-H' complex (red) and for H' DNA only (black), at 100 mM KCl (**A**) and 200 mM KCl (**B**); the intensities in each panel have been normalized to match at the lowest temperature. The donor intensity in the DNA only samples reflects the change in the donor quantum yield as a function of temperature. (**C,D**) An enlarged region of interest from (**A,B**). The vertical lines indicate the initial (T_i) and final (T_f)

temperatures corresponding to the respective T-jump relaxation traces shown in (**E,F**). The horizontal lines indicate the corresponding donor intensities of the complex, denoted by $I_c^{eq}(T_i)$ and $I_c^{eq}(T_f)$, and of the reference (H' DNA only) sample, denoted by $I_{ref}^{eq}(T_i)$ and $I_{ref}^{eq}(T_f)$. (**E,F**) Representative relaxation kinetics traces in response to a T-jump perturbation for the IHF-H' complex at 100 mM KCl (**E**) and 200 mM KCl (**F**). The horizontal dashed lines indicate the fluorescence intensity levels $I(0^-)$, $I(0^+)$ and $I(\infty)$ as defined in Eq. S3. The magnitude of the T-jump in each relaxation trace is estimated by comparing the initial drop in the T-jump traces with the equilibrium temperature dependence of the donor fluorescence of the reference sample. The value of T_f such that $\frac{I(0^+)}{I(0^-)} = \frac{I_{ref}^{eq}(T_f)}{I_{ref}^{eq}(T_i)}$ is assigned as the final temperature after the T-jump for that kinetics trace. The amplitude of the relaxation trace, determined by the increase in the intensity from $I(0^+)$ to $I(\infty)$ (see Eq. S2), is determined by the equilibrium temperature dependence of the donor fluorescence in the complex sample such that $\frac{I(\infty)}{I(0^-)} = \frac{I_c^{eq}(T_f)}{I_c^{eq}(T_i)}$.

Figure S5. Comparison of single-exponential, double-exponential, and MEM fits to T-jump relaxation traces of IHF-H' in 100 mM KCl. (**A,B**) The kinetics traces shown are the same as in Figure 2 of the main text, but the data points have been averaged further here for clarity. In each panel, the continuous green (blue) line is a fit to a single-exponential (double-exponential) decay function convoluted with the T-jump recovery; the continuous red line, which is the corresponding fit using the MEM analysis and is also shown in main text Figure 2, is not easily discerned from the from the double-exponential (blue) fit. Residuals are plotted from single-exponential fits (**C,D**), from double-exponential fits (**E,F**) and from MEM fits **(G,H)**.

Figure S6. Comparison of double-exponential and MEM analysis on IHF-H'. (**A**) The relaxation rates for the fast (pink) and slow (gray) phases, calculated using the double-exponential decay function convoluted with T-jump recovery (Eq. S3), are plotted as a function of inverse (final) temperature. The open and closed symbols represent two independent sets of measurements. The relaxation rates and the error bars in each set were obtained from a Monte Caro search in parameter space, as described in Supplementary Methods 1.7. The dashed lines are an Arrhenius fit to the relaxation rates, with activation energies −2.5 ± 1.4 kcal/mol (fast phase) and 5.1 ± 1.6 kcal/mol (slow phase). The Arrhenius fits were done for the two data sets combined, and the errors in the activation energies are standard deviations of values obtained from independent fits to the two sets of measurements. (**B**) The corresponding relative amplitudes for the fast (pink) and slow (gray) phases, obtained from the double-exponential fits, are shown. The dashed lines connect the data points and are drawn to guide the eye. (**C**) The average relaxation rates from the discrete-exponential (Monte Carlo) analysis, averaged over the two data sets (pink and gray symbols) are plotted versus the inverse (final) temperature, together with the corresponding rates from the MEM analysis (green and blue symbols). The dashed lines are Arrhenius fits to the discrete-exponential results (as in panel **A**); the continuous lines are Arrhenius fits to

the MEM results. (**D**) The corresponding comparison of relative amplitudes obtained from double-exponential and MEM analyses. The MEM results in panels (**C,D**) are identical to those presented in Figure 3 of the main text.

Figure S7. Control T-jump experiments to rule dye dynamics as contributing to relaxation kinetics. (**A**) Donor fluorescence emission intensities of donor-only labeled H' samples in the presence of IHF, with excitation of donor at 488 nm, measured in response to a T-jump perturbation, are plotted as a function of time. (**B**) Acceptor fluorescence emission intensities of donor-acceptor labeled H' in complex with IHF, with direct excitation of acceptor at 536 nm, measured in response to a T-jump perturbation. (**C**) Donor fluorescence emission intensities of donor-acceptor labeled 14-mer DNA oligonucleotide, with excitation of donor at 488 nm, measured in response to a T-jump perturbation. (**D**) Sequence of the 14-bp construct; nucleotides indicated in green are identical to the nucleotides next to the dyes in the longer H' sequence. The FRET E measured for this DNA construct was 0.48 ± 0.05, similar to the FRET E of 0.57 ± 0.02 in the IHF-H' complex.

Figure S8. Comparison of T-jump relaxation kinetics measured on IHF-H' and IHF-H'55 complexes. (A,B) Donor fluorescence emission intensities of double-labeled H' (35-bp) and a longer (55-bp substrate containing the H' site) in the presence of IHF, measured in response to a T-jump perturbation, are plotted as a function of time in (**A**) and (**B**), respectively. Red continuous lines are fits to the relaxation traces from the MEM analyses, as described in the text. (**C,D**) Control measurements on free fluorescein samples are also shown. Red continuous lines are fits to the T-jump recovery function, with recovery time constant fixed at $\tau_{\mathrm{rec}} \approx 210\ \mathrm{ms}$. **(E,F)** The distribution of relaxation times that best fit the relaxation traces in (**A**) and (**B**) are plotted in (**E**) and (**F**), respectively. The blue continuous lines in (**F**) are fits to the distributions in terms of two Gaussians (green), with independently varied peak positions and widths, as described in the text. The amplitudes of the two phases obtained from the MEM distributions are 22% (fast) and 78% (slow) for IHF-H', and 30% (fast) and 70% (slow) for IHF-H'55, for similar T-jump perturbation conditions, as indicated in panels (**A**) and (**B**).

Figure S9. T-jump kinetics measurements on IHF-TT8AT in 100 mM KCl. (**A,B**) Donor fluorescence emission intensities of double-labeled TT8AT samples in the presence of IHF measured in response to a T-jump perturbation are plotted as a function of time, for two different T-jump conditions. Red continuous lines are fits to the relaxation traces from the MEM analyses, as described in the text. (**C,D**) Control measurements on free fluorescein samples are also shown. Red continuous lines are fits to the T-jump recovery function, with recovery time constant fixed at $\tau_{\mathrm{rec}} \approx 210\ \mathrm{ms}$. **(E,F)** The distribution of relaxation times that best fit the relaxation traces in (**A**) and (**B**) are plotted in (**E**) and (**F**), together with the fits to the distributions in terms of two Gaussians, as described in Supplementary Figure S1C.

Figure S10. Comparison of single-exponential, double-exponential, and MEM fits to T-jump relaxation traces of IHF-TT8AT in 100 mM KCl. (**A,B**) The kinetics traces shown are

the same as in Supplementary Figure S9, but the data points have been averaged further here for clarity. Each panel is as described in Supplementary Figure S5.

Figure S11. Comparison of double-exponential and MEM analysis on IHF-TT8AT. Each panel is as described in Supplementary Figure S6. The MEM results in panels (**C,D**) are identical to those presented in Figure 4A,B of the main text.

Figure S12. T-jump kinetics measurements on IHF-TTloop in 100 mM KCl. Each panel is as described in Supplementary Figure S9.

Figure S13. T-jump kinetics measurements on IHF-ATloop in 100 mM KCl. Each panel is as described in Supplementary Figure S9.

Figure S14. T-jump kinetics measurements on IHF-H'44A in 100 mM KCl. Each panel is as described in Supplementary Figure S9.

Figure S15. MEM analysis of relaxation traces measured on a single time-scale. (A,B) Donor fluorescence emission intensities of double-labeled H'44A samples in the presence of IHF measured in response to a T-jump perturbation are plotted as a function of time, for two different T-jump conditions. These data were measured on a single time-scale and hence have not been scaled and matched. Red continuous lines are a fit using the MEM analysis. (**C,D**) Control measurements are shown on donor-only strand of the H'44A sequence. Red continuous lines are fits to the T-jump recovery function (Eq. S6), with recovery time constant fixed at $\tau_{\mathrm{rec}} = 210$ ms. **(E,F)** The distribution of relaxation times that best fit the relaxation traces in (**A**) and (**B**) are plotted in (**E**) and (**F**), respectively (red). Note that, even for T-jump traces measured on a single time-scale, the MEM analysis still reveals two components in the distribution.

Figure S16. Equilibrium melting profiles of H' and IHF-H' for varying salt concentrations. The donor intensity of donor-acceptor-labeled H' DNA-only sample (black) and IHF-H' sample (red) versus temperature are shown for measurements in 50 mM KCl (**A**), 100 mM KCl (**B**), 150 mM KCl (**C**), and 200 mM KCl (**D**). The data demonstrate that the extent of DNA unbending in the IHF-H' complex as the temperature is raised is larger at higher [salt].

Figure S17. T-jump kinetics measurements on IHF-H' in 50 mM KCl. Data in each panel are as described in Supplementary Figure S9. Panel (**G**) shows the donor intensity of the H' DNA-only sample (black) and IHF-H' sample (red) versus temperature, similar to the data shown in Figure 1D of the main text. The open symbols in each set represent reversibility checks and were measured after the sample was heated up to 60 °C and then cooled back down to 20 °C.

Figure S18. T-jump kinetics measurements on IHF-H' in 150 mM KCl. Each panel is as described in Supplementary Figure S17.

Figure S19. T-jump kinetics measurements on IHF-H' in 200 mM KCl. Each panel is as described in Supplementary Figure S17.

Figure S20. Comparison of relaxation rates and relative amplitudes for the IHF-H' complex in 50 mM and 100 mM KCl. (**A**) The relaxation rates for the fast (green) and slow (blue) phases, measured in 50 mM KCl, are plotted as a function of inverse temperature. (**B**) The corresponding relative amplitudes for the fast (green) and slow (blue) phases are shown. The dashed lines in each panel represent the data measured in 100 mM KCl, reproduced from Figure 3 of the main text.

Figure S21. T-jump kinetics measurements on αK5A-H' in 100 mM KCl. Each panel is as described in Supplementary Figure S9.

Figure S22. T-jump kinetics measurements βK84A-H' in 100 mM KCl. Each panel is as described in Supplementary Figure S9.

Figure S23. T-jump kinetics measurements αR21C-H' in 100 mM KCl. Each panel is as described in Supplementary Figure S9.

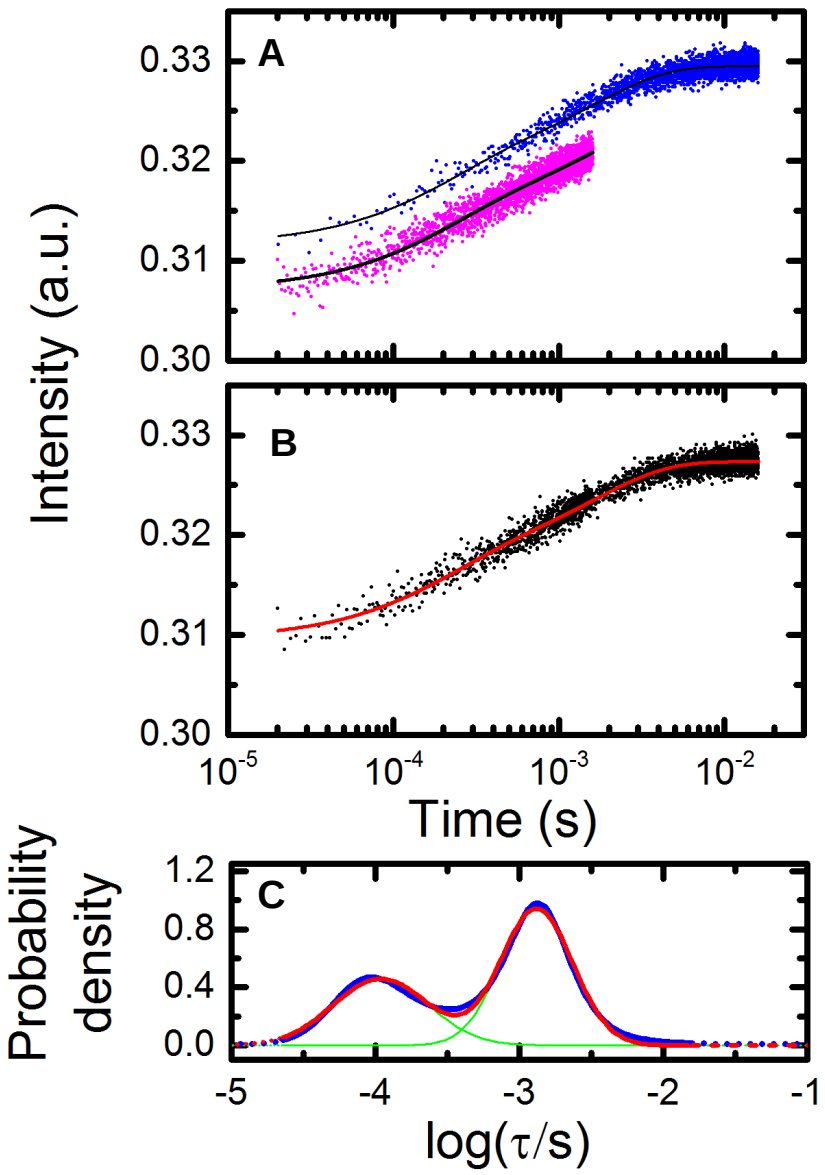

Supplementary Figure S1

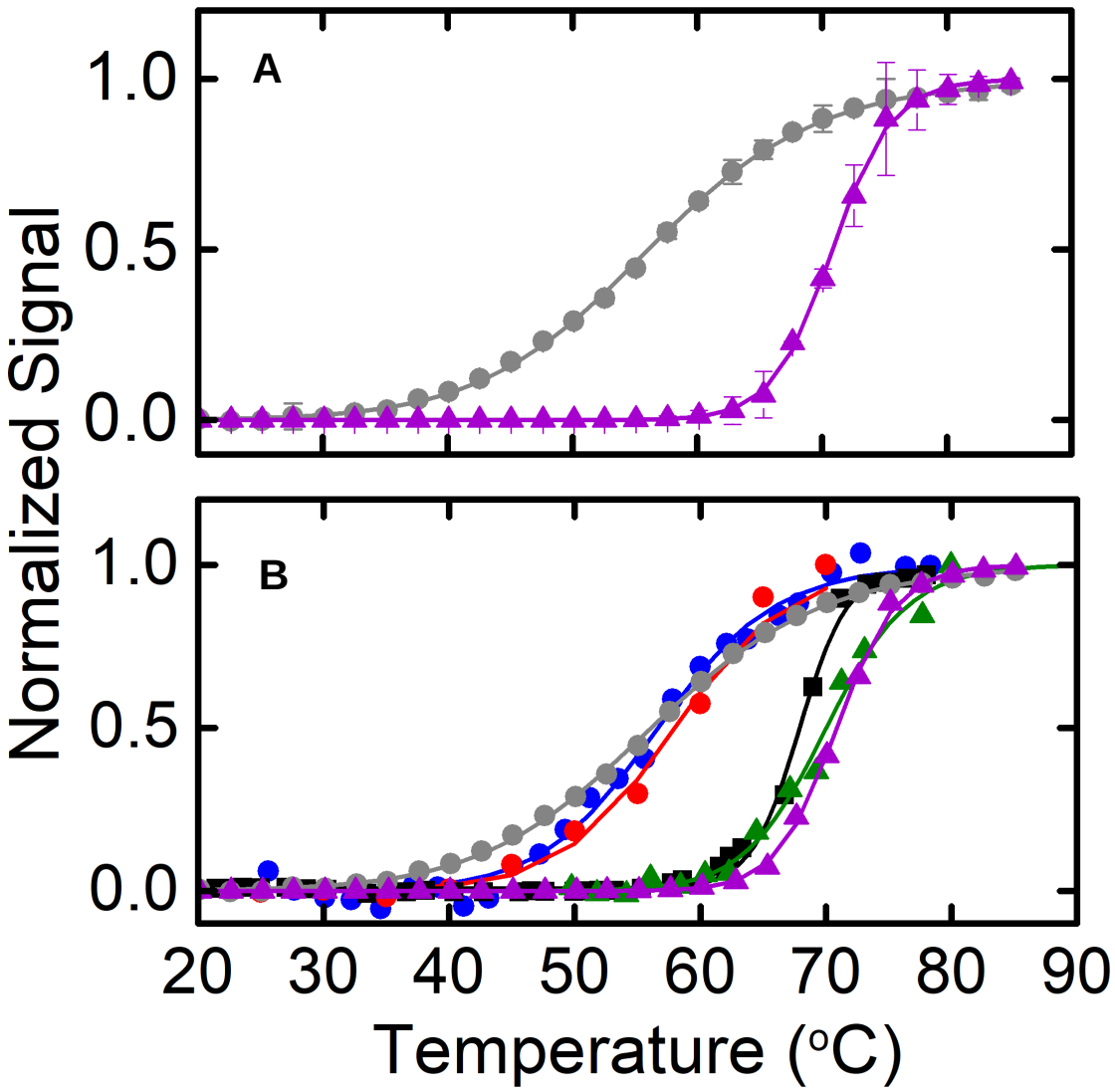

Supplementary Figure S2

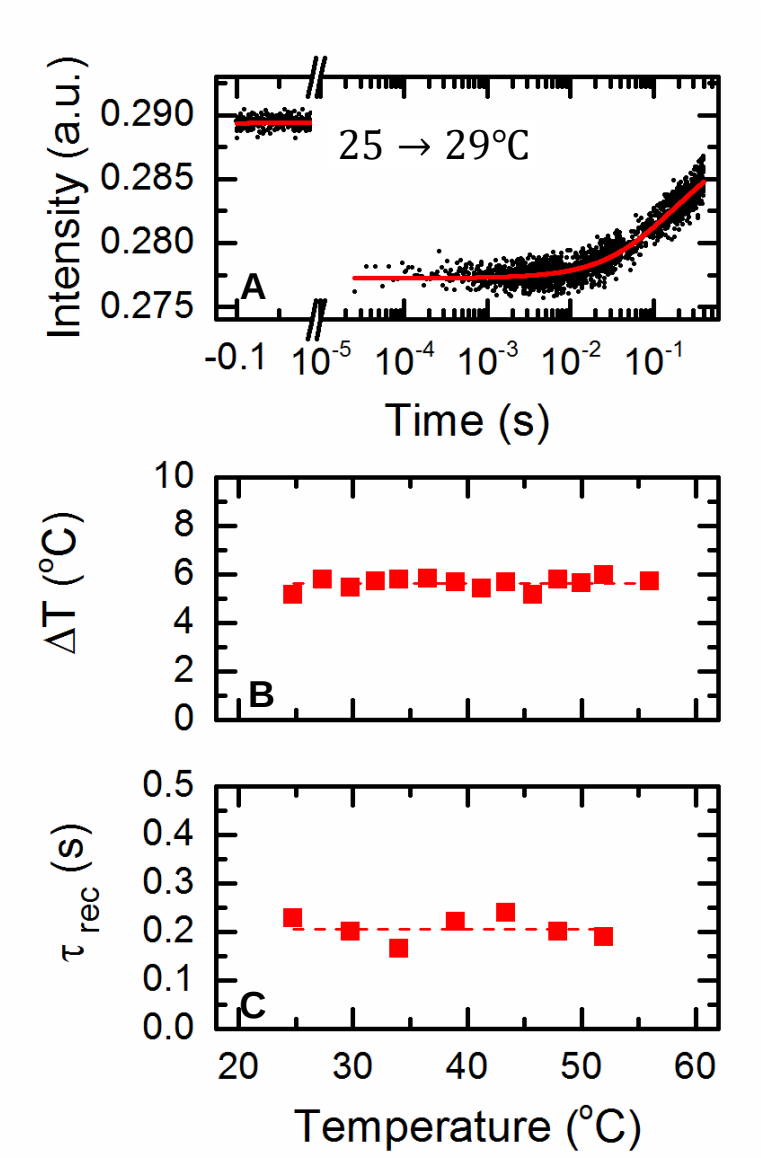

Supplementary Figure S3

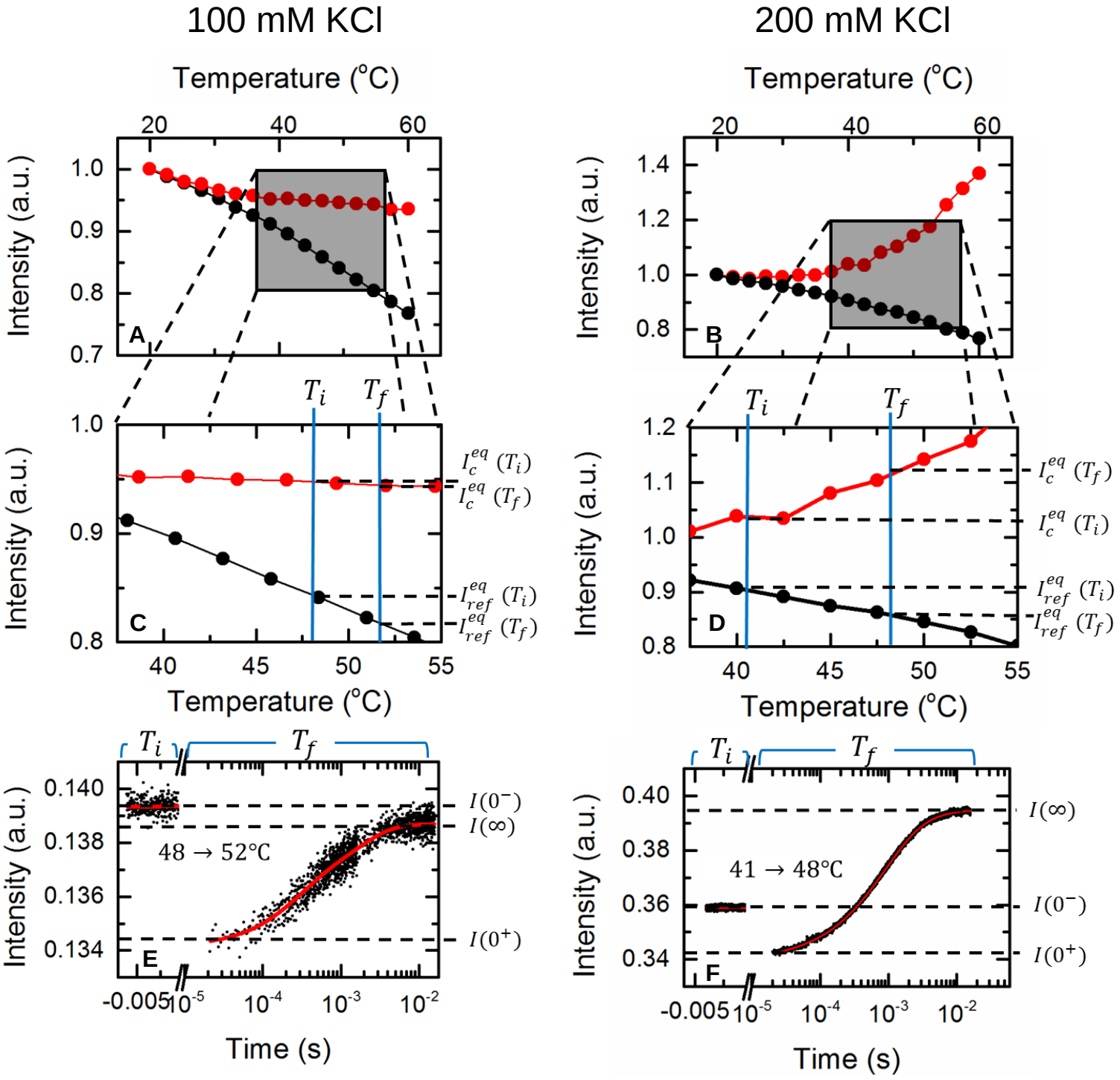

Supplementary Figure S4

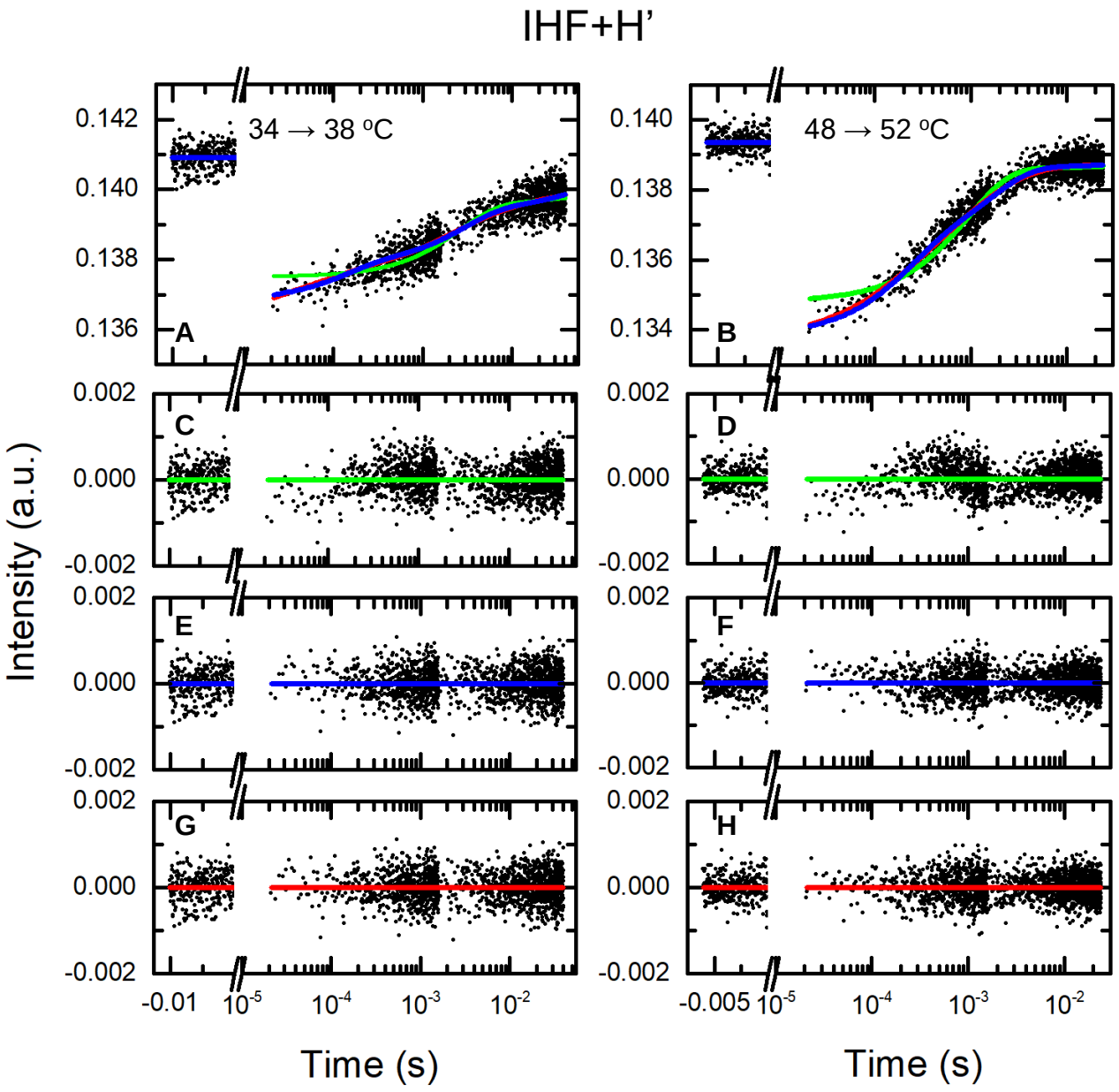

Supplementary Figure S5

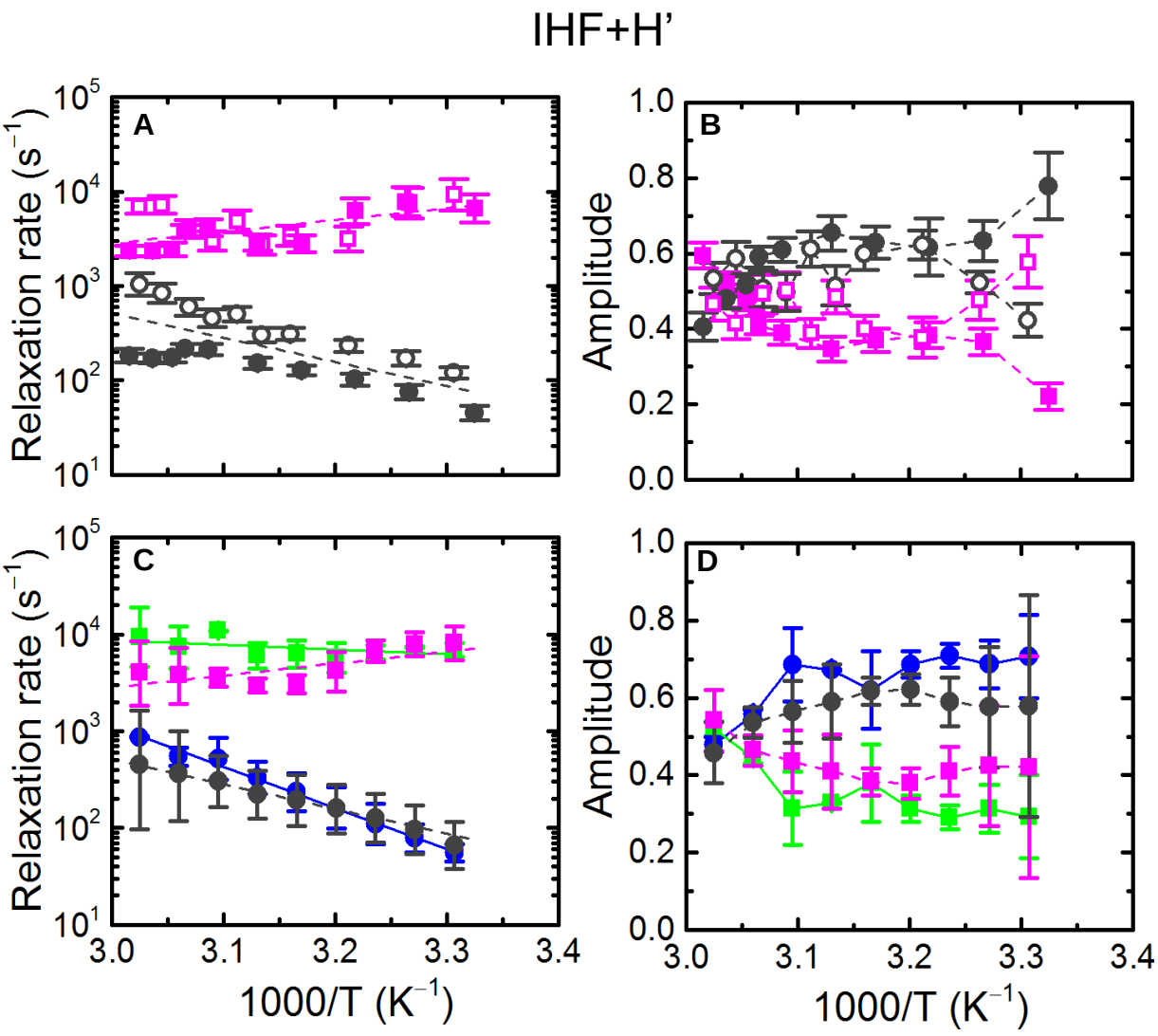

Supplementary Figure S6

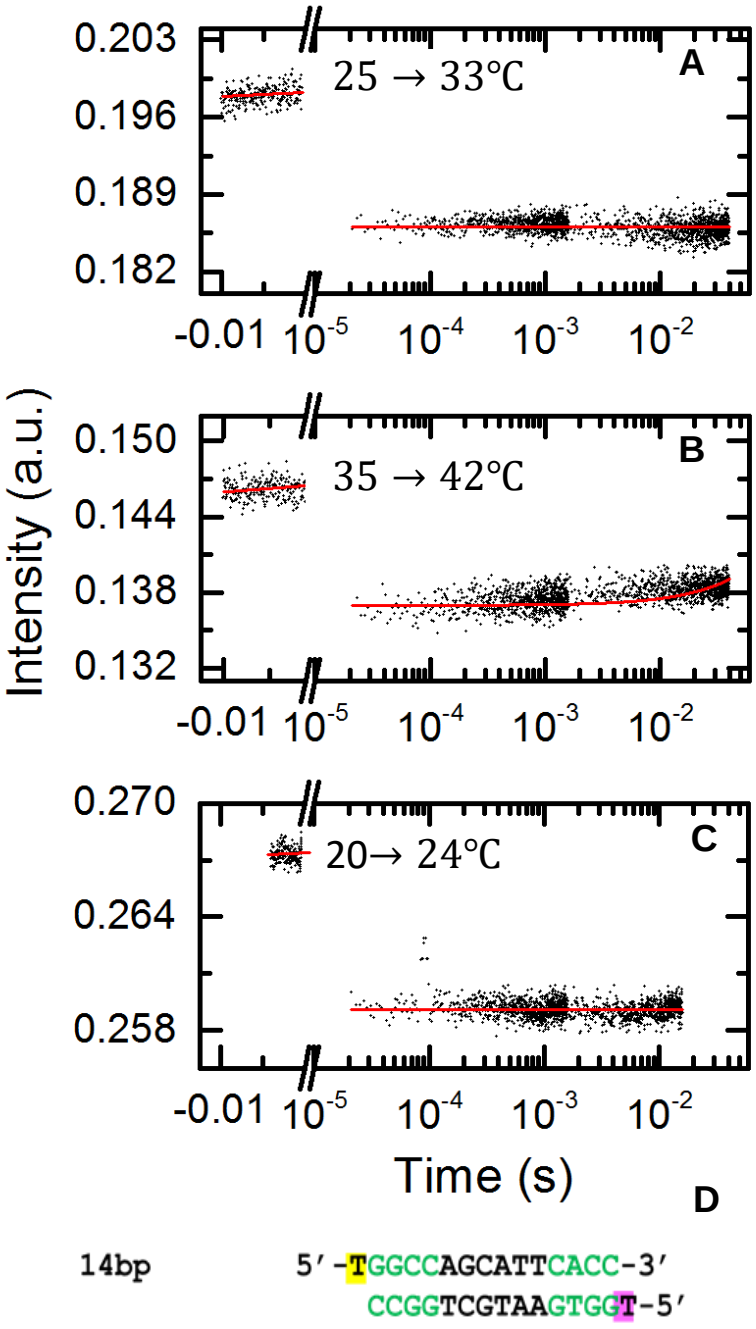

Supplementary Figure S7

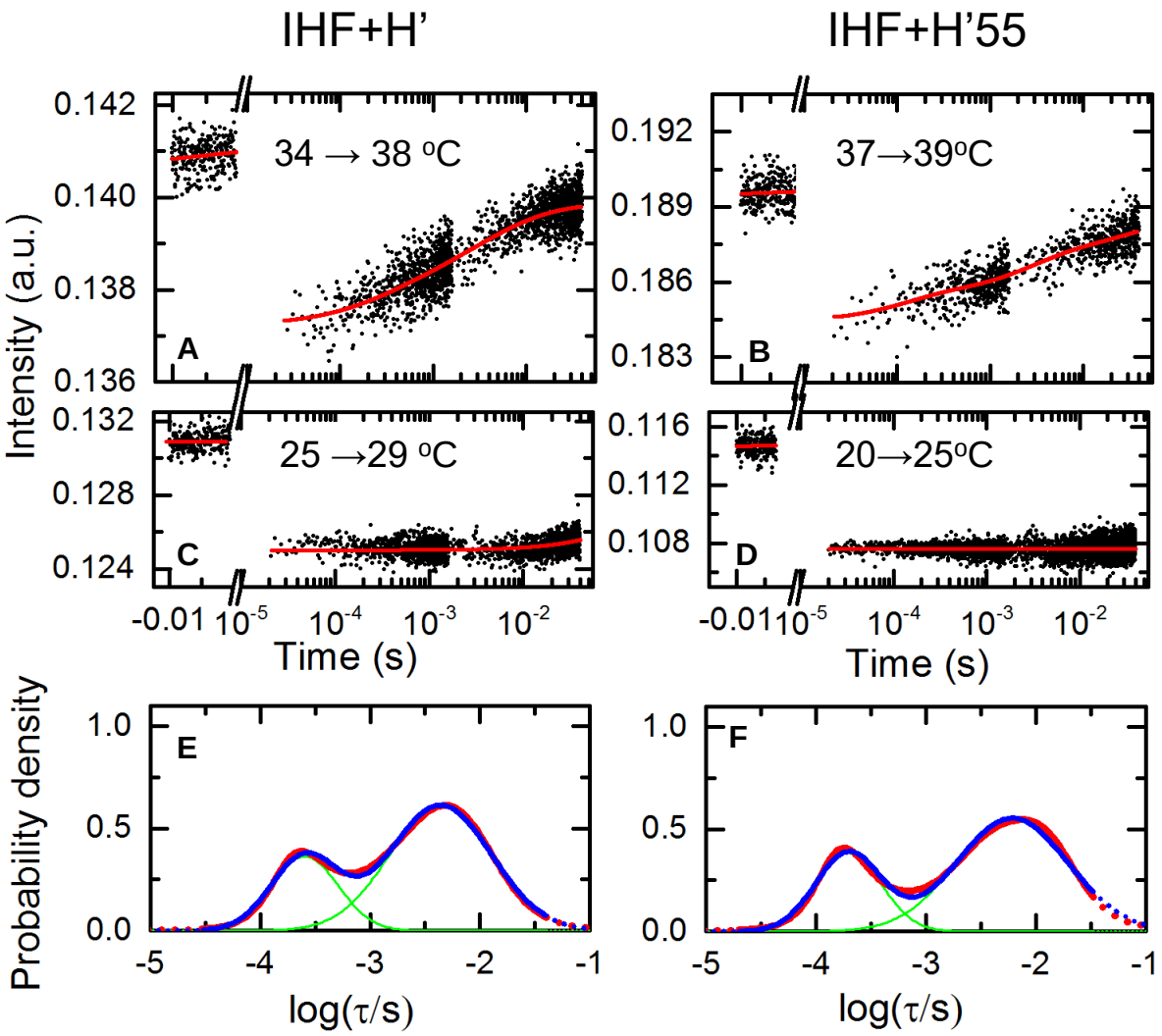

Supplementary Figure S8

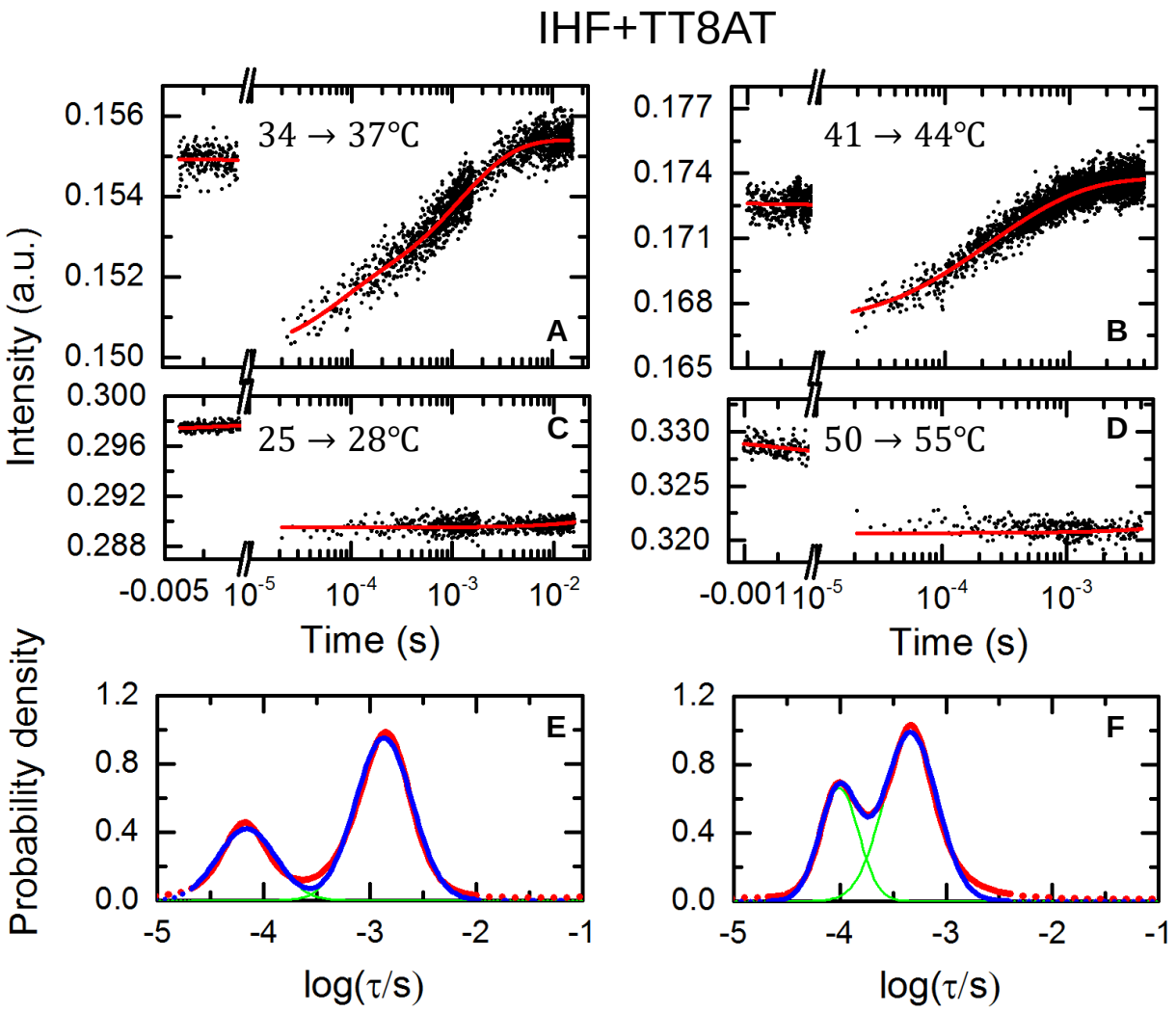

Supplementary Figure S9

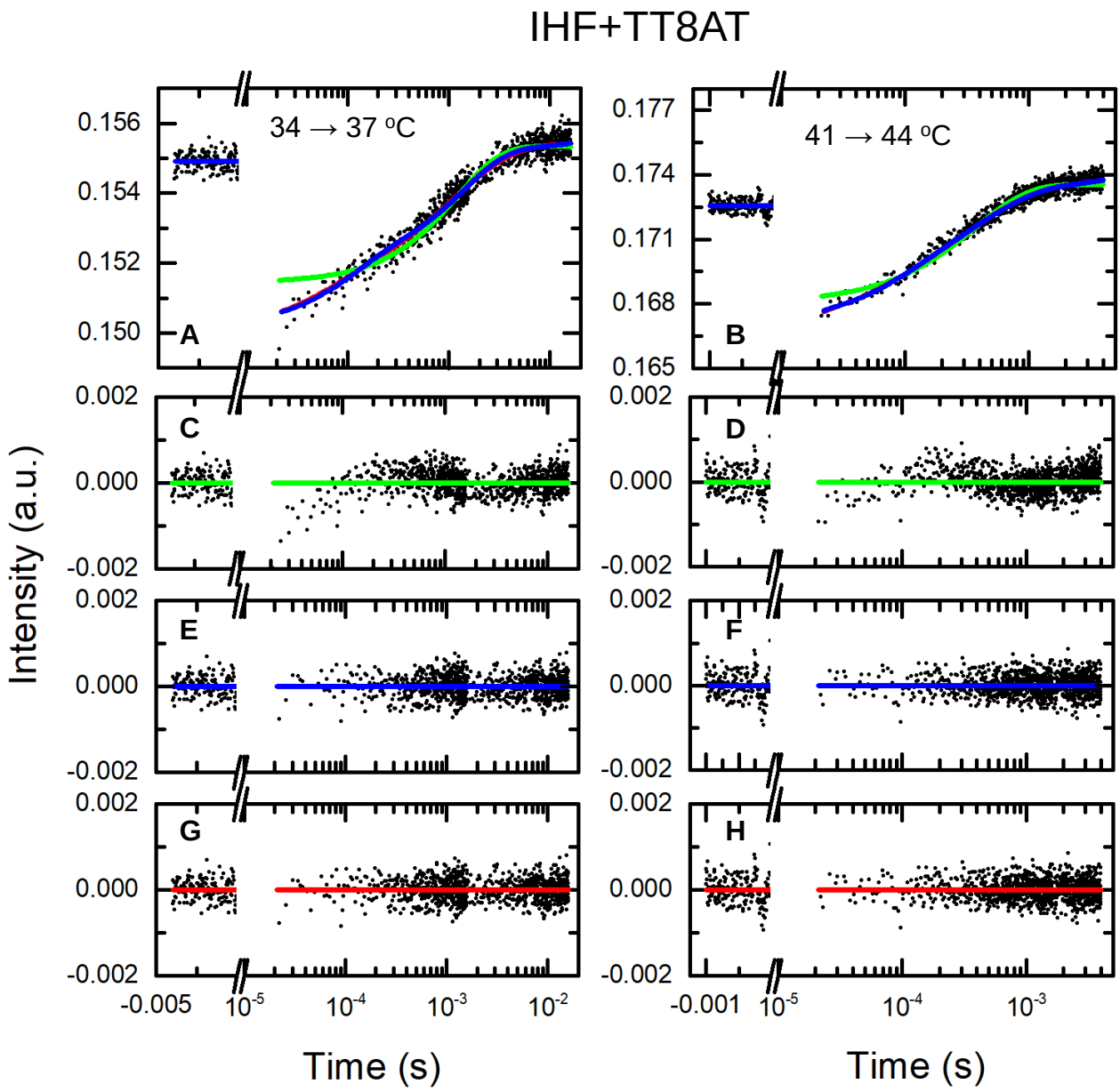

Supplementary Figure S10

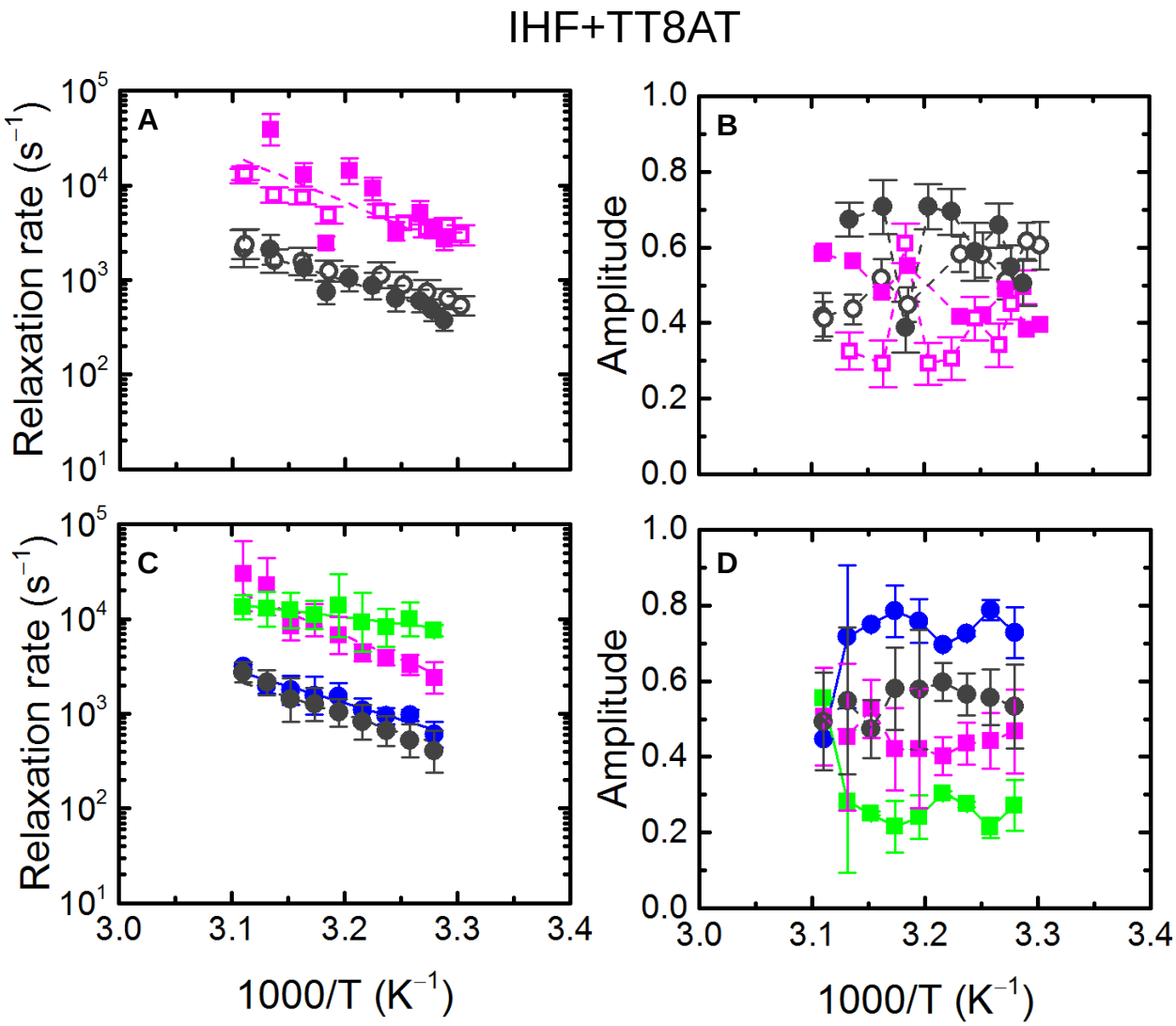

Supplementary Figure S11

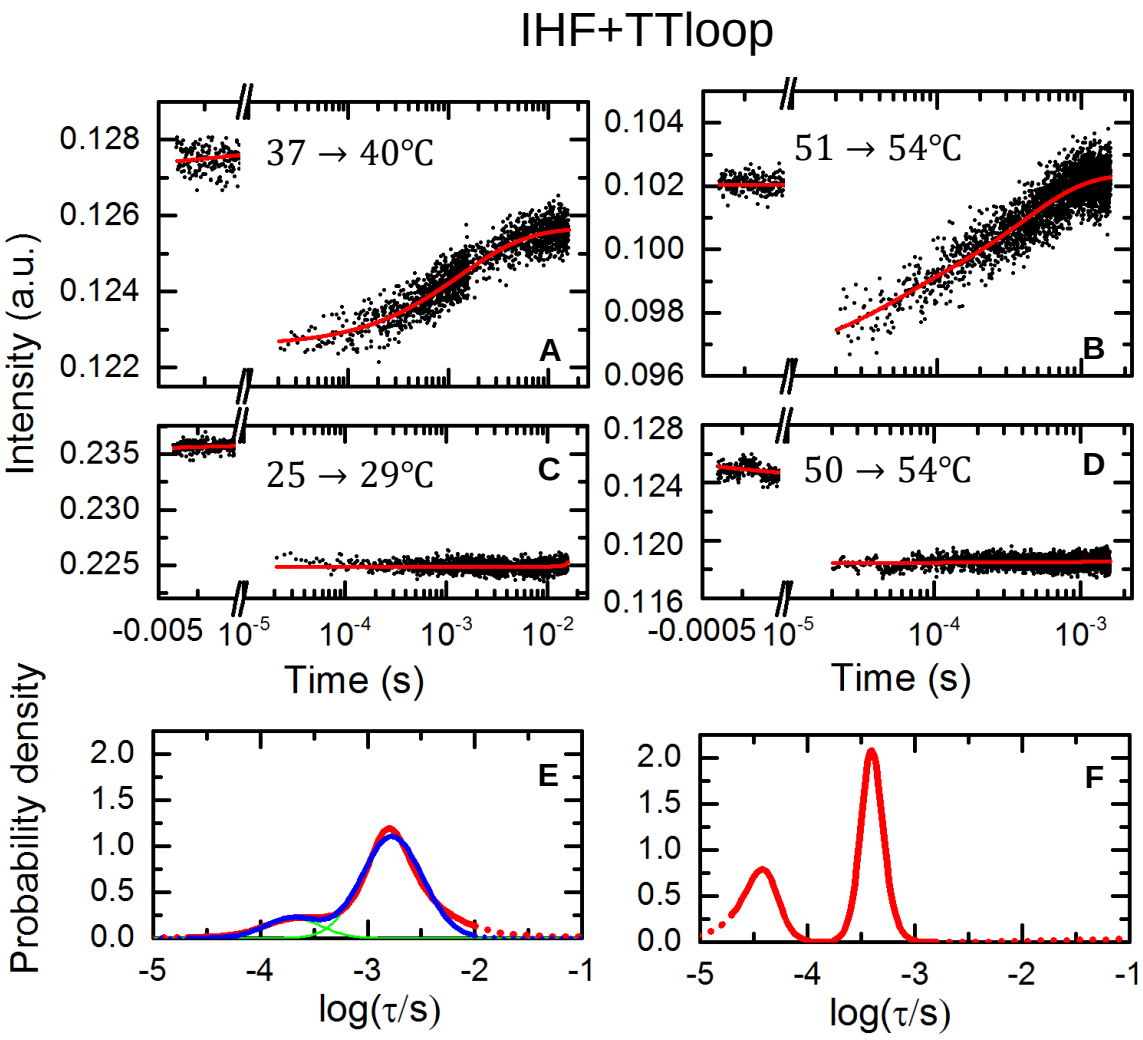

Supplementary Figure S12

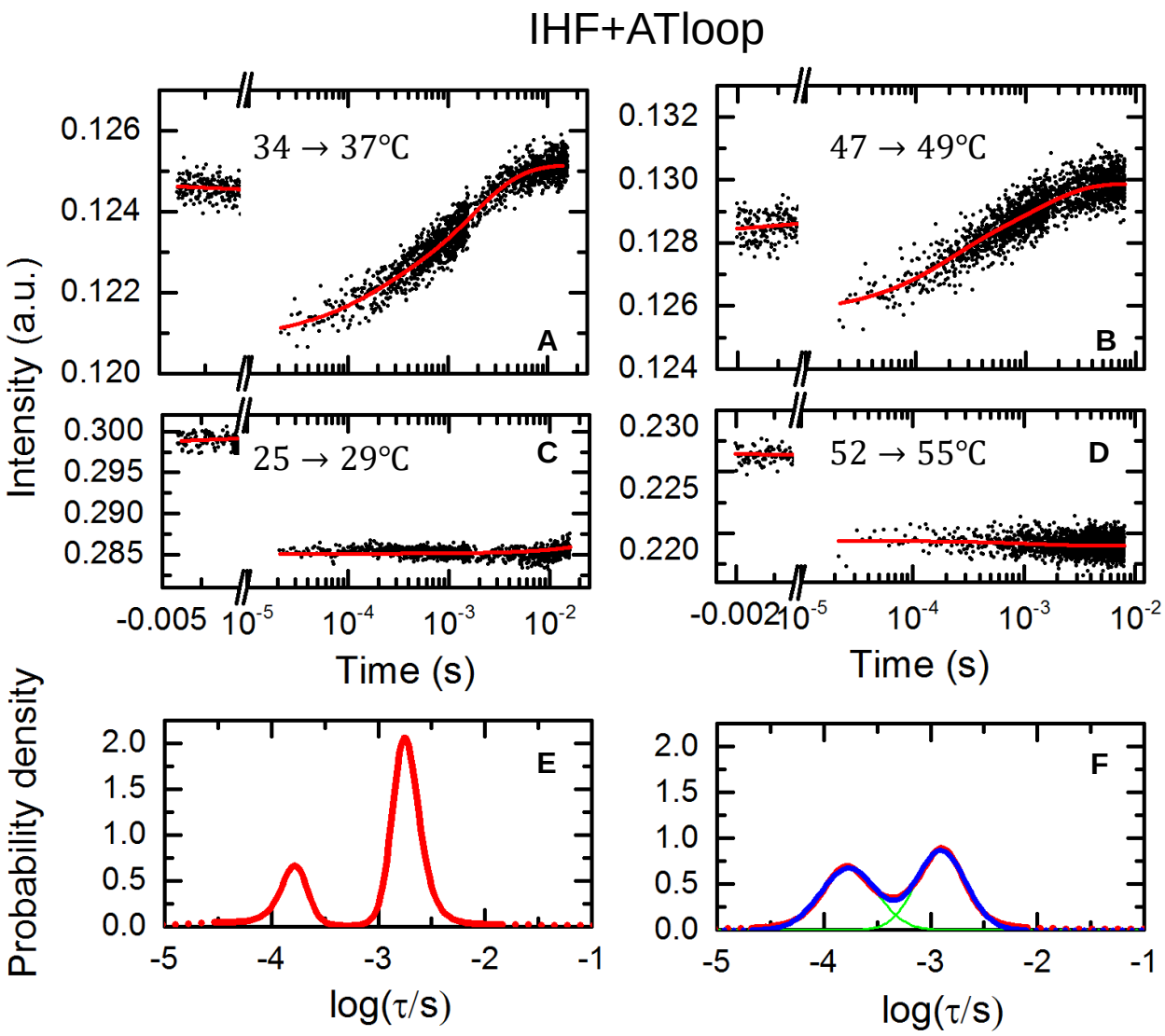

Supplementary Figure S13

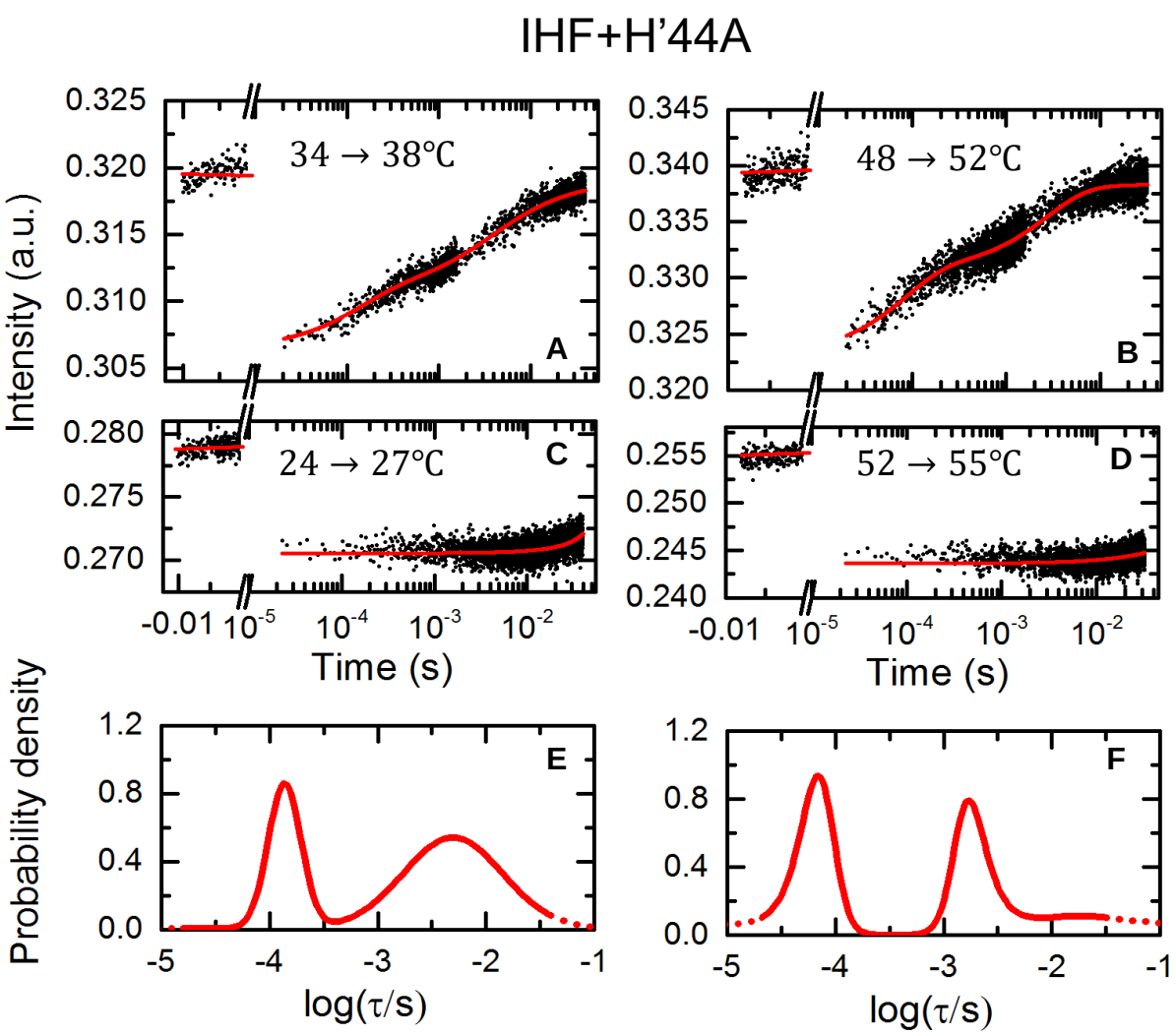

Supplementary Figure S14

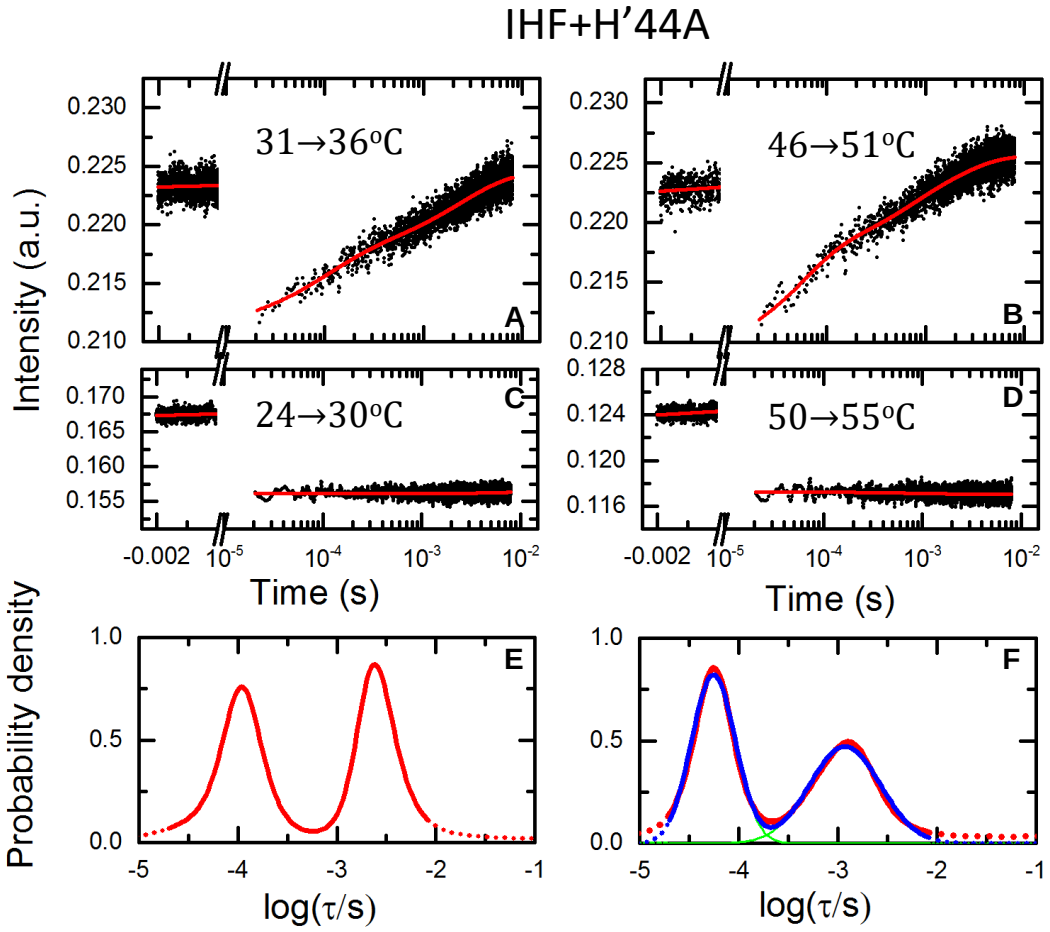

Supplementary Figure S15

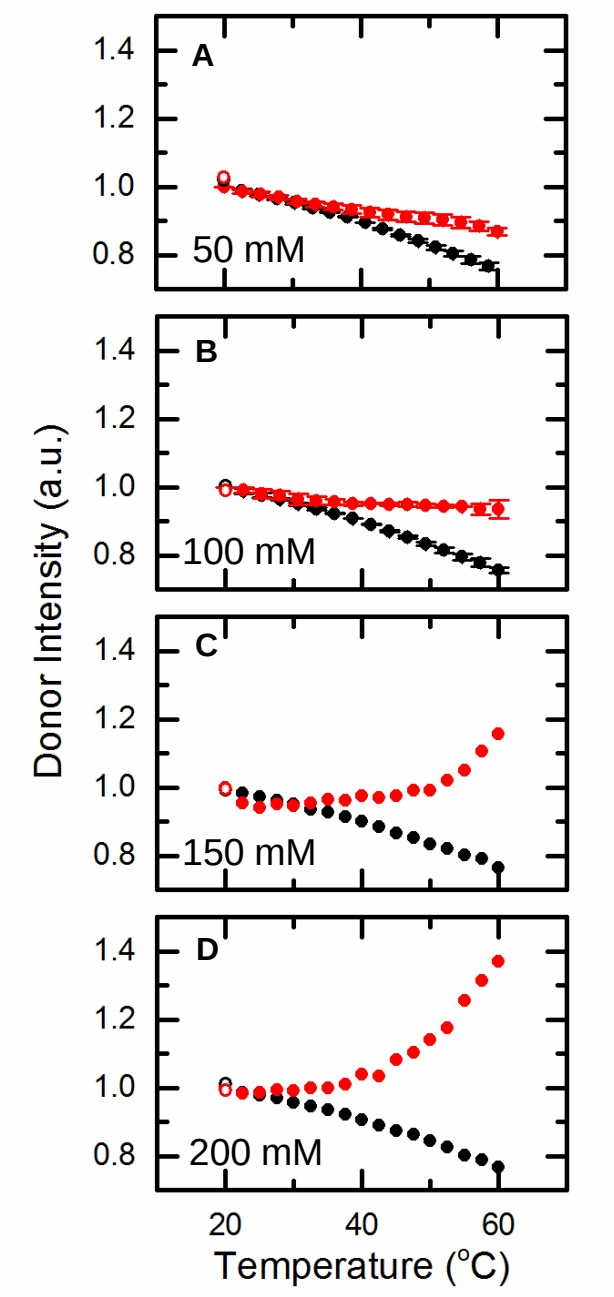

Supplementary Figure S16

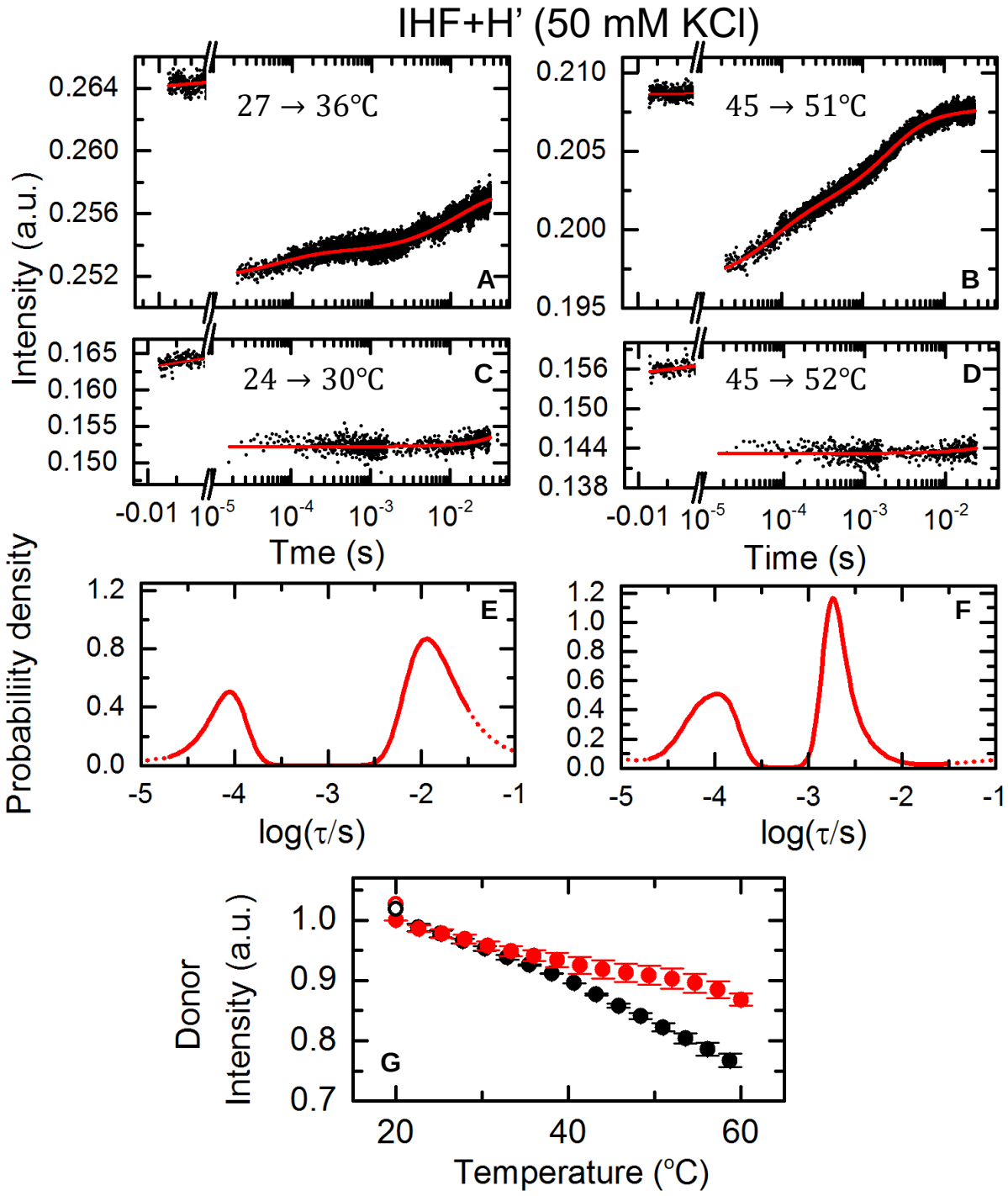

Supplementary Figure S17

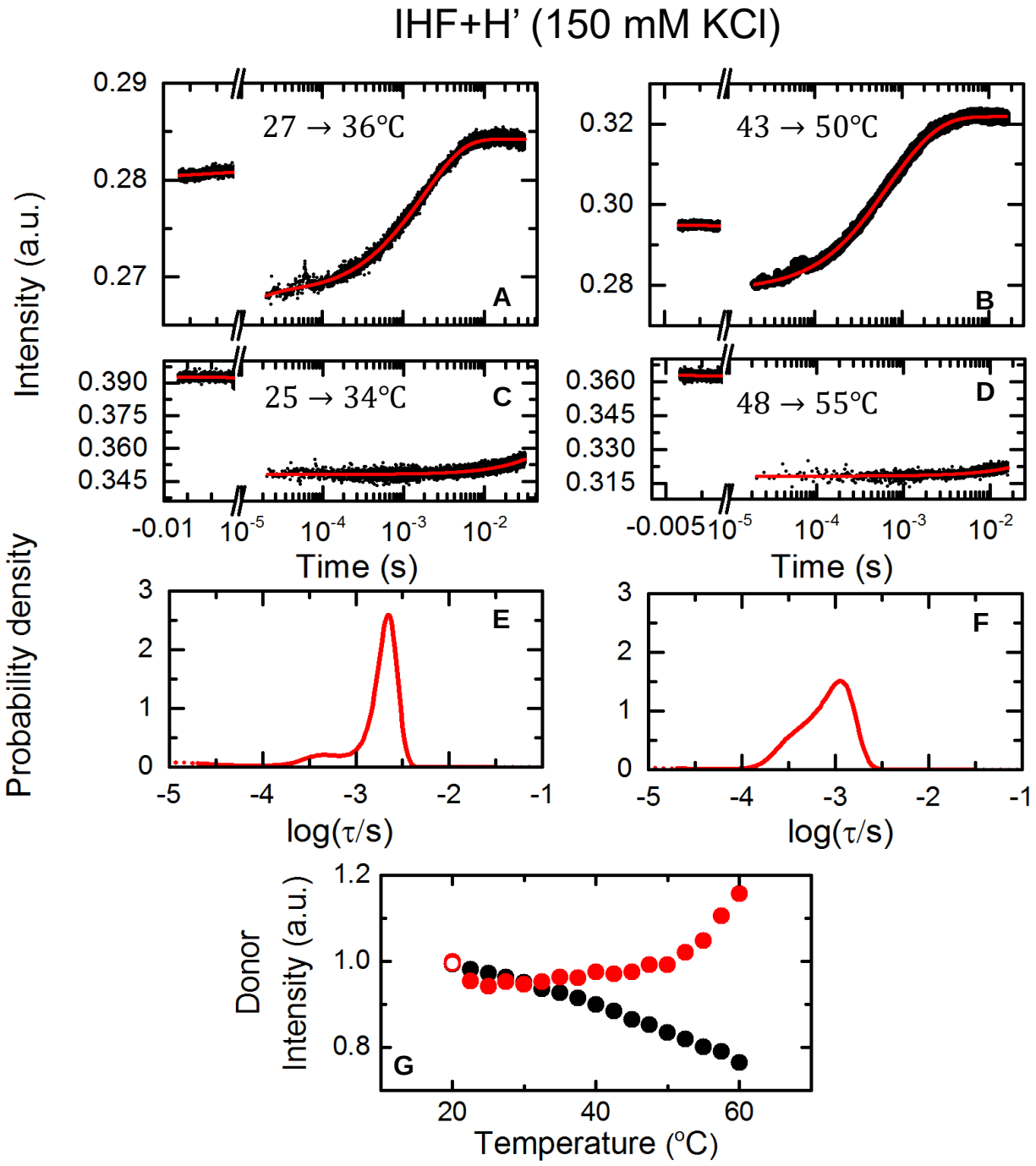

Supplementary Figure S18

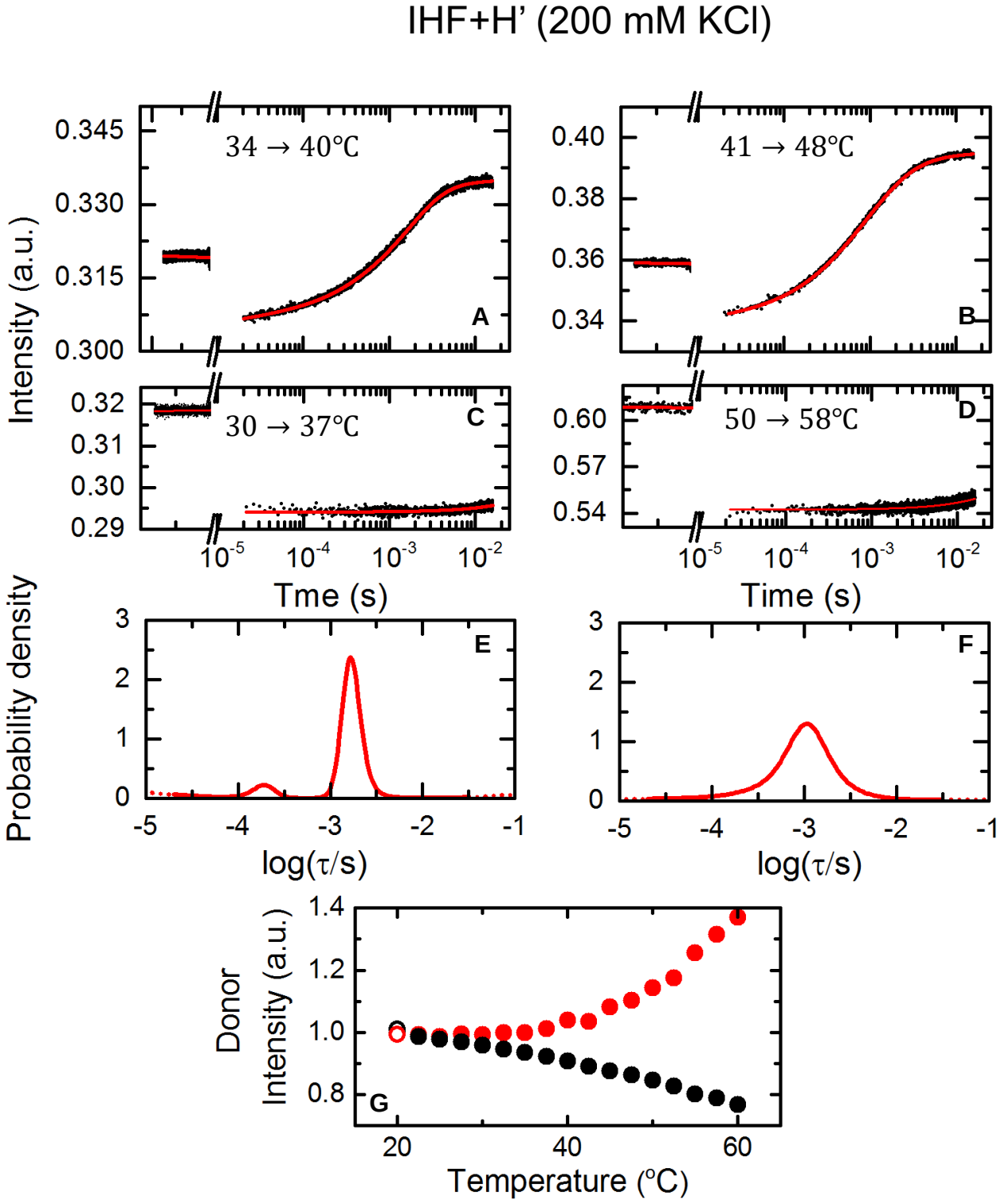

Supplementary Figure S19

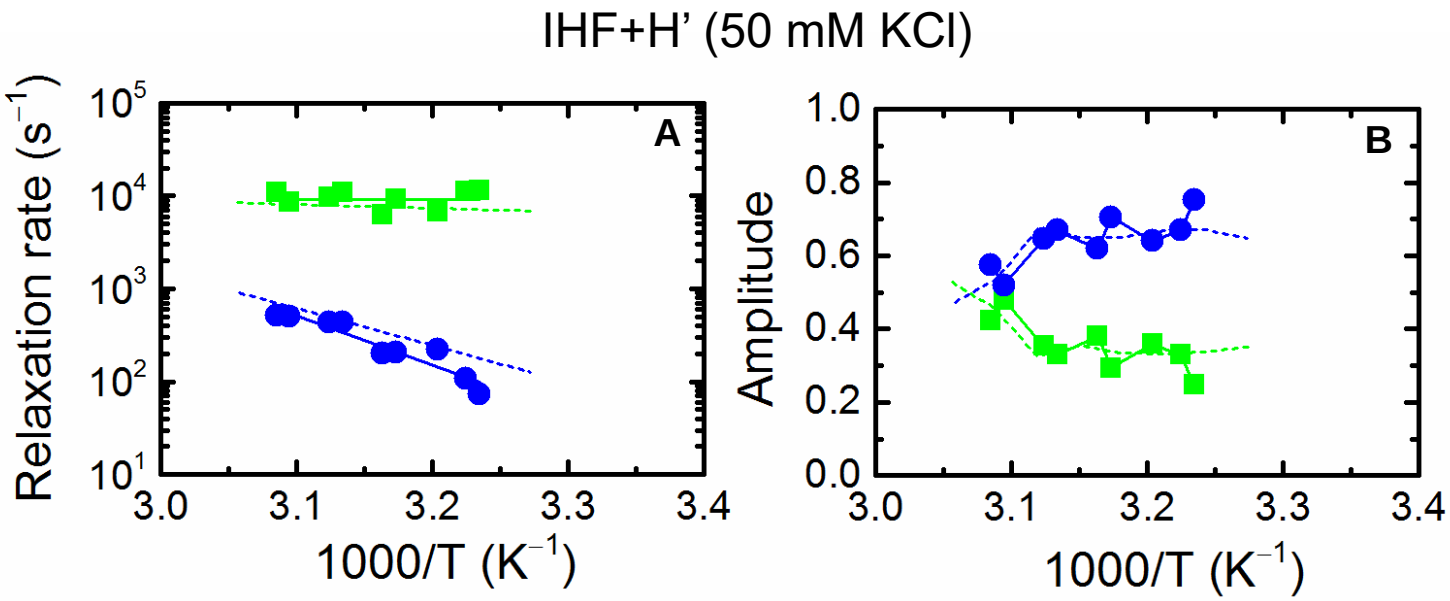

Supplementary Figure S20

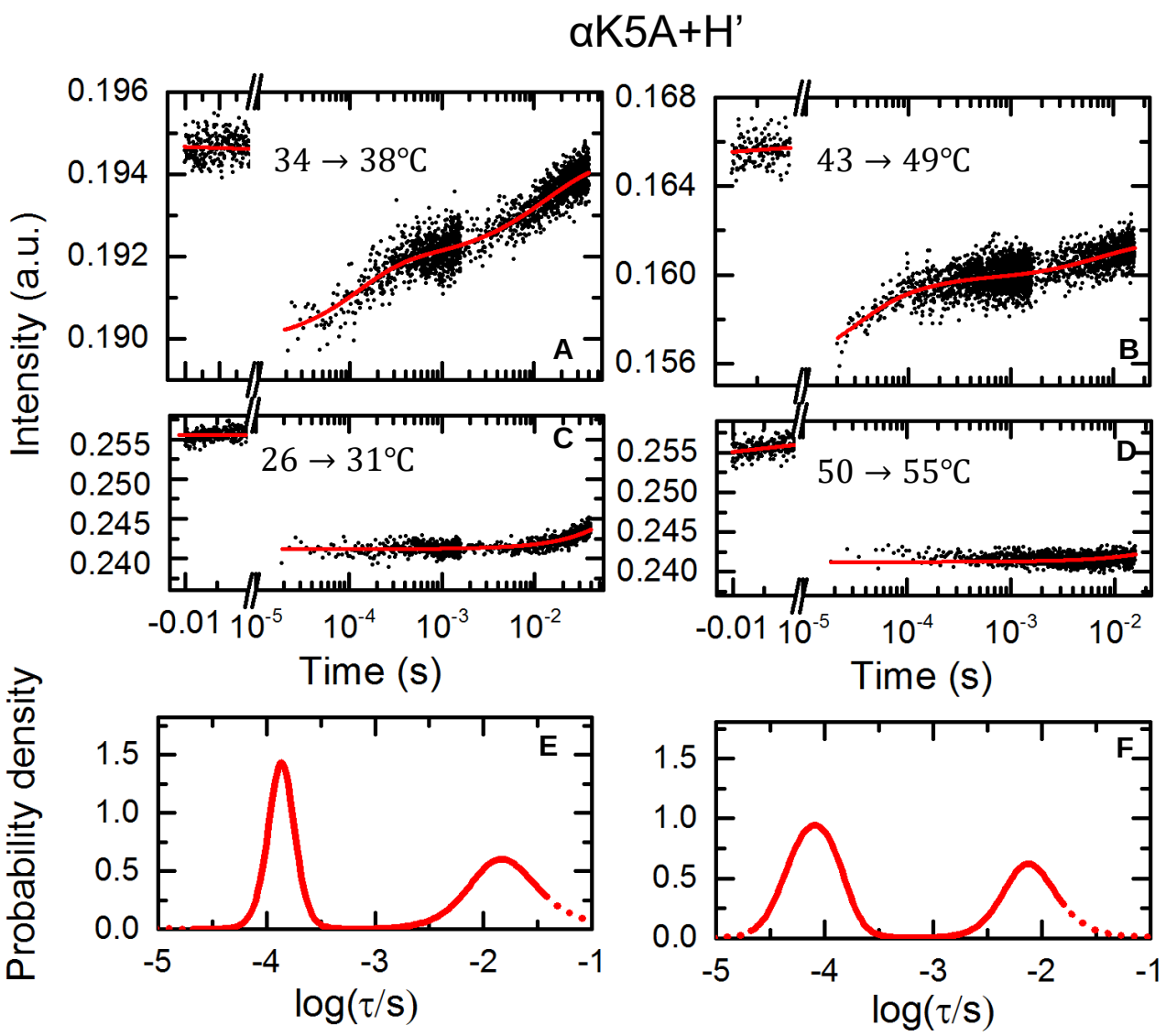

Supplementary Figure S21

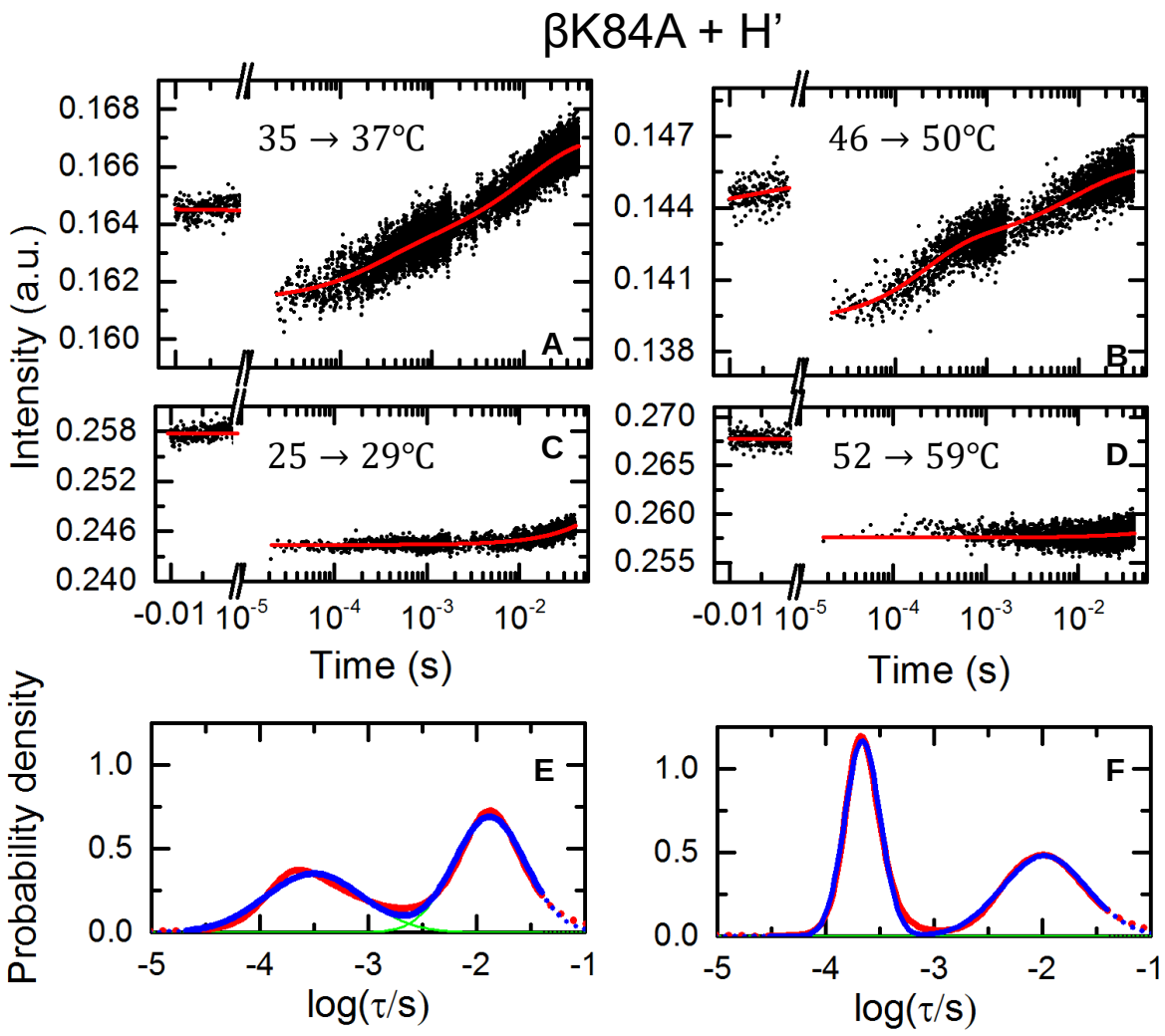

Supplementary Figure S22

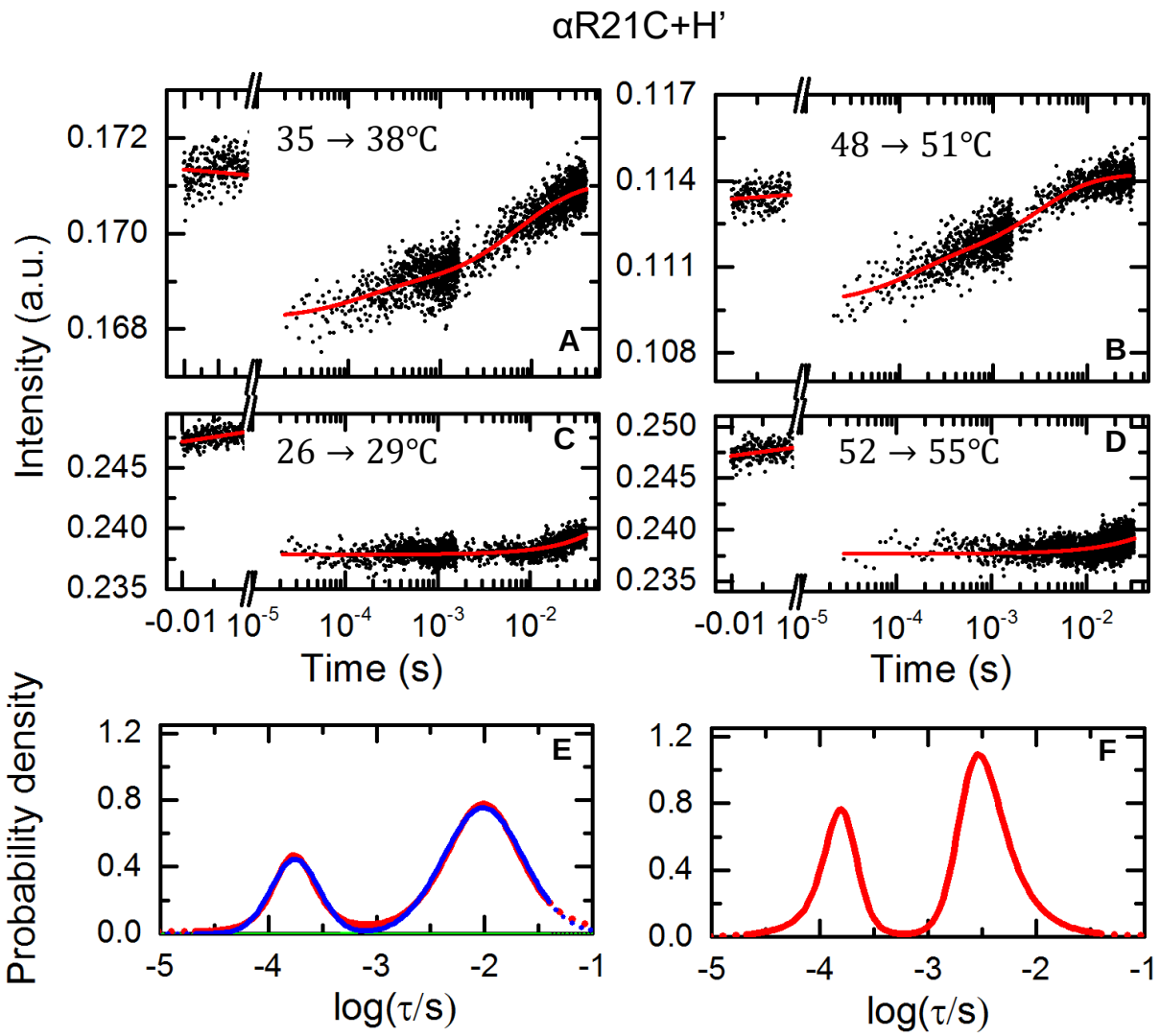

Supplementary Figure S23